Electronic Supplementary Material (ESI) for Polymer Chemistry.
This journal is © The Royal Society of Chemistry 2023

Supporting Information

Inverse Vulcanisation of Self-Activating Amine and Alkyne Crosslinkers

Liam Dodd, William Sandy, Romy Dop, Bowen Zhang, Amy Lunt, Daniel R. Neill, Tom Hasell

Department of Chemistry, University of Liverpool, Crown St, Liverpool, L69 7ZD, United Kingdom

Table of Contents

I. General Considerations

All chemicals were used as received. All Chemicals were obtained from Sigma Aldrich unless otherwise specified. Ground sulfur sublimed powder reagent grade ≥99.5 % was obtained from Brenntag UK & Ireland. Triallylphosphine 97+% and triallylphosphite were obtained from thermo scientific. Triallylphosphate >96%, Dicyclopentadiene (stabilised with BHT) [precursor to Cyclopentadiene] >97%, and 1,3-Diisopropenylbenzene (stabilised with TBC) >97% were obtained from Tokyo Chemicals Industry. Prop-2-yn-1-amine 98% was obtained from Manchester organics. CHNS combustion microanalyses were performed on an elementar Vario Micro cube, with a first analysis performed to acquire rough data that was then used to calibrate the instrument for a second, more accurate analysis. Differential scanning calorimetry was performed on a TA instruments DSC25 discovery series equipped with an RCS90 and using Tzero aluminium hermetic pans and aluminium lids, in the heating range -90 °C to 150 °C, at a heating rate of 15 °Cmin^{-1} and a cooling rate of 7.5 °Cmin^{-1}. PXRD data were collected in transmission mode on a Panalytical X'Pert PRO MPD equipped with a high throughput screening (HTS) XYZ stage, X-ray focusing mirror and PIXcel detector, using Cu Kα radiation. Data were measured on loose powder samples held on thin Mylar film in stainless steel well plates, over the range 4 to 40 ° in approximately 0.013 ° steps over 60 minutes. All calculations were performed using the Gaussian 09 code. The following method has previously been found to be effective for the prediction of vibrational spectra, and so was used here: an initial energy minimisation using MMFF molecular mechanics was performed before geometry optimisation and energy calculation using the BP86 functional with the Def2-TZVPP basis set, applying a D3(BJ) empirical dispersion correction. FT-IR spectra were obtained on a Bruker vertex 70 diamond ATR. All TGA data was obtained on a TA instruments TGA550, operating under nitrogen with a ramp rate of 20 °Cmin^{-1} using platinum pans equipped with disposable aluminium cups. For the battery testing, samples were held isothermal at 350 °C for 1 hour.

II. Reaction Methods

II.A. Standard Dispersion Polymerisation

Mass X of sulfur was added to 50 cm^3 of xylene, which was then heated to reflux with 200 rpm stirring from a 14 mm cross shaped stirrer. Mass Y of a chosen crosslinker was then added to the reaction, where mass X plus mass Y always equalled 10 g in every reaction. The stirring was then increased to 1400 rpm, and the reaction was left at reflux overnight. This afforded two products: an insoluble fraction of polymer, and a soluble fraction of polymer. The two were separated by filtration, and the insoluble fraction, which often remained stuck to the sides of the reaction vessel, was removed by embrittlement via direct addition of liquid nitrogen and scraping with a spatula. The soluble fraction of polymer was evaporated to dryness, and then cured overnight in an oven at 140 °C to give what was termed, the sol product, of which it is important to note, may no longer be soluble in xylene and other solvents due to reacting and crosslinking further upon curing. The insoluble fraction of the reaction was purified by Soxhlet extraction on toluene overnight, after which it was cured in an oven at 140 °C to give what was termed, the insol product. The products of these reactions will be referred to by the following naming convention: NAMEα-Sβ-X, where NAME is the abbreviation of the crosslinker in use, α is the feed ratio of that crosslinker in the reaction, β is the feed ratio of sulfur in that reaction, and X is replaced with either sol, to refer to the sol product, or insol, to refer to the insol product. Polymers were stored in the freezer at -20 °C, as Dale et al. has shown that the aging of inverse vulcanised polymers can be delayed by cold storage.

The above optimised method was reached after several iterations where several variables were modified. It was found that reaction volumes of 25, 50, and 100 mL of xylene had negligible effect on the reactions, and so 50 mL was chosen as the best compromise between convenient extraction and efficient use of solvent. With a 50 mL reaction volume, the presence of sodium dodecyl sulfate as a surfactant was tested, in weights of 0.01, 0.1, and 1 gram in a reaction, which was found to have negligible effect on the reaction.

II.B. Dispersion Polymerisations of Low Boiling Point Crosslinkers

The method for polymerising MPA and DAA had to be modified, as these crosslinkers boil at below the melting temperature of sulfur (83 °C for MPA and 111 °C for DAA). To account for this, MPA and DAA were reacted as described in Section II.A., but at the initial temperatures of 70 °C and 100 °C, respectively. After 24 hours, a pre-polymer had formed. Attempting to cure this pre-polymer in the oven as detailed in Section II.A. an auto-acceleration resulted. As such, the reaction was continued in a dispersion polymerisation method, but after the initial 24 hours at 70 °C or 100 °C, the temperature was then increased to reflux, and left to react overnight. Other than this modification, the method remained the same as in Section II.A..

II.C. Dispersion Polymerisation of Phosphorus Compounds

The method for polymerising the phosphorus containing crosslinkers, TAPIN, TAPIT, and TAPAT was the same as the method in section II.A. with the exception that these reactions needed longer to go to completion. Thus, once the crosslinker had been added to the reaction mixture, the reaction was left for one week rather than one day. The Sol and Insol products were also left to cure for two days to ensure the curing process was complete.

II.D. Bulk Polymerisation Method for Crosslinker Blends

All reactions were performed in triplicate upon a hotplate equipped with an aluminium heating pan and an aluminium heating block, which ensured consistent positioning of the reaction vials upon the hotplate, giving consistent stirring. To a 40 mL reaction vial, a 14 mm cross-shaped stirrer was added. The mass was then recorded. A desired amount of elemental sulfur (5.0000 g for a reaction with DCPD, and 3.0000 g for a reaction with linseed oil), weighed out to within 0.0050 g of the target mass, was then added to the reaction vial. The reaction vial was heated to 135 °C, such that the sulfur melted. At least ten minutes for thermal equilibration was then allowed, with 200 rpm stirring during. Then, approximately 17 g of DCPD or 23 g of linseed oil (the exact masses were recorded) were added to a vial. Note that 17 g of DCPD was sufficient for three reactions each containing 5 g of DCPD, and that 23 g of linseed oil was sufficient for three reactions each containing 7 g of linseed oil. Using the exact mass of crosslinker recorded, the appropriate mass of either TAA or TPA was added to the crosslinker and thoroughly mixed to make a stock solution that would constitute the appropriate concentration of TAA or TPA to give the following mass percentages when added to the molten sulfur: 49 % DCPD and 1 % TAA or TPA, 47 % DCPD and 3 % TAA or TPA, 69 % linseed oil and 1 % TAA or TPA, 67 % linseed oil and 3 % TAA or TPA. For a DCPD reaction 5.0000 g ± 0.0050 g of the chosen stock solution was added to a new vial. This vial was then tared, and its contents added to the molten sulfur in the reaction vial, then re-weighing the empty vial to find the exact amount of stock solution added to the reaction by means of weighing by difference. For a linseed oil reaction 7.0000 g ± 0.0050 g of the chosen stock solution was added to a new vial. This vial was then tared, and its contents added to the molten sulfur in the reaction vial, then re-weighing the empty vial to find the exact amount of stock solution added to the reaction by means of weighing by difference. Once the stock solutions were added to the reaction vials, the reaction vials were immediately sealed with a septum with an affixed air balloon, and the stirring was increased to 800 rpm (any faster resulted in flicking of droplets the reaction mixture to the top of the vial). The time of the addition of the stock solution was noted. The air balloon was for pressure regulation, but also prevented volatilised crosslinker from escaping, thereby minimising crosslinker evaporation as volatilised crosslinker was unable to escape. The reactions were monitored closely, and the time at which the reaction mixture became so viscous that the stirrer could no longer rotate was noted. The time elapsed between addition of the stock solution and the ceasing of stirring was noted as the vitrification time. The reaction vials were then left on the hotplate at 135 °C for two days to cure. The septum and balloon were then removed, and the reaction vial was re-weighed to determine the yield, after which the glass vial was cooled with liquid nitrogen to detach the polymer from the vial. The vial was then shattered to retrieve the polymer. The polymer was then shattered to retrieve the stirrer.

III. Proposed Mechanism for Nucleophilic Initiation

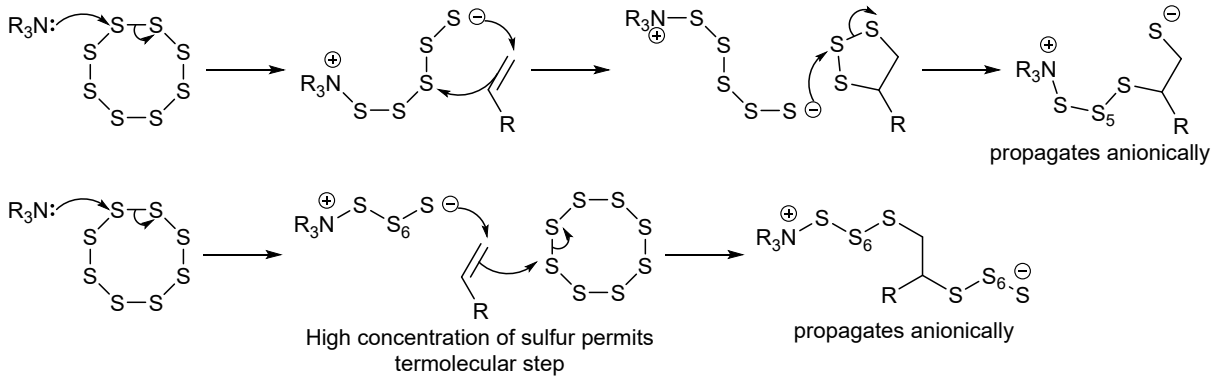

Figure S1: Proposed mechanism for anionic initiation of an inverse vulcanisation reaction by nucleophilic activation via amine activator.

IV. Representative TGA Data

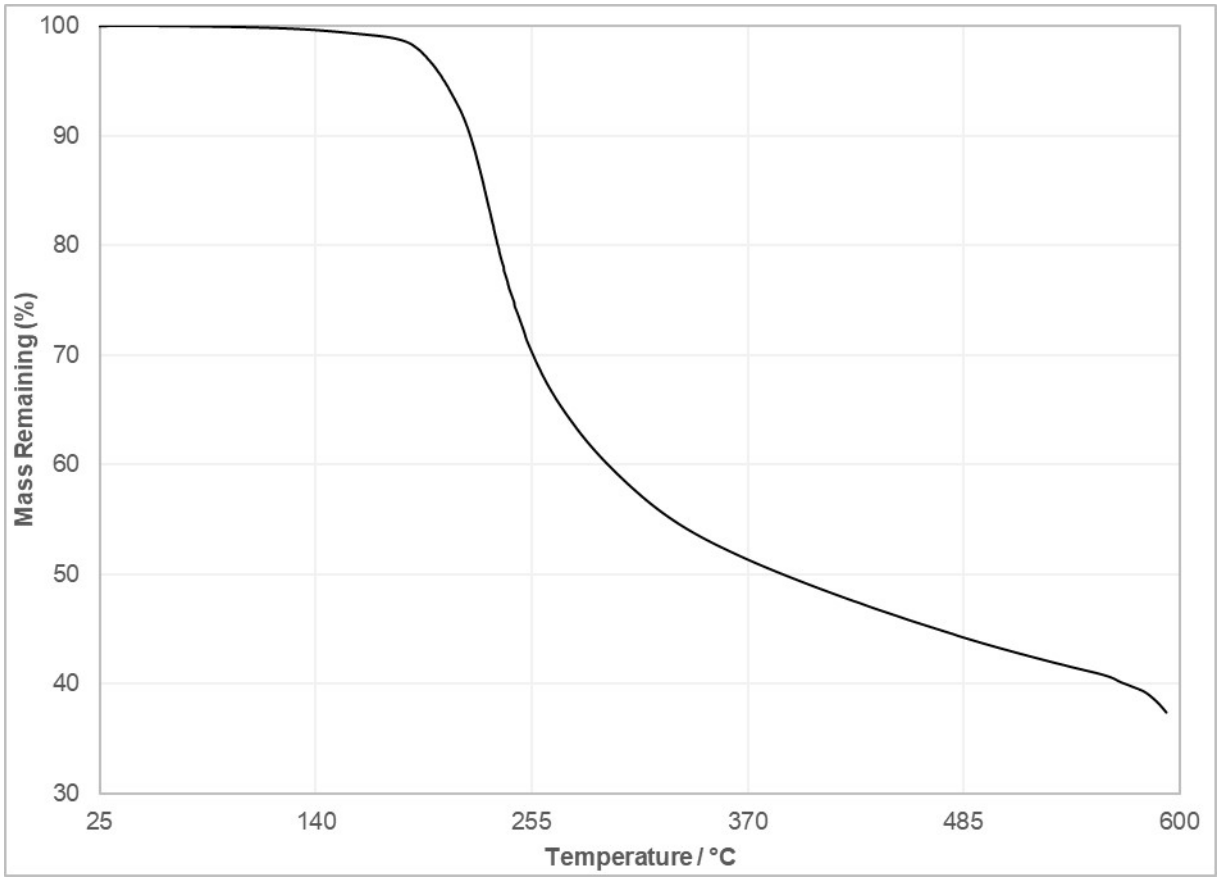

Figure S2: The TGA trace of TAA50-S50-Insol.

Table S1: Decomposition temperatures obtained from TGA for certain polymers

Polymer	Insol T_d / °C	Sol T_d / °C
TPA70-S30	209.8	227
TPA50-S50	210.3	196.2
TPA30-S70	214.9	211.4
TPA10-S90	213.9	221
TPA5-S95	209.6	223.4
TAA70-S30	206.7	218.8
TAA50-S50	198.5	214.3
TAA30-S70	194.2	215.3
TAA10-S90	194.3	215.6
TAA5-S95	210.2	222.1
NON70-S30	217.5	209.8
NON50-S50	218.3	204.9
NON30-S70	213.4	212.2
NON10-S90	217	220
NON5-S95	219.8	224.4

V. Representative DSC Thermograms

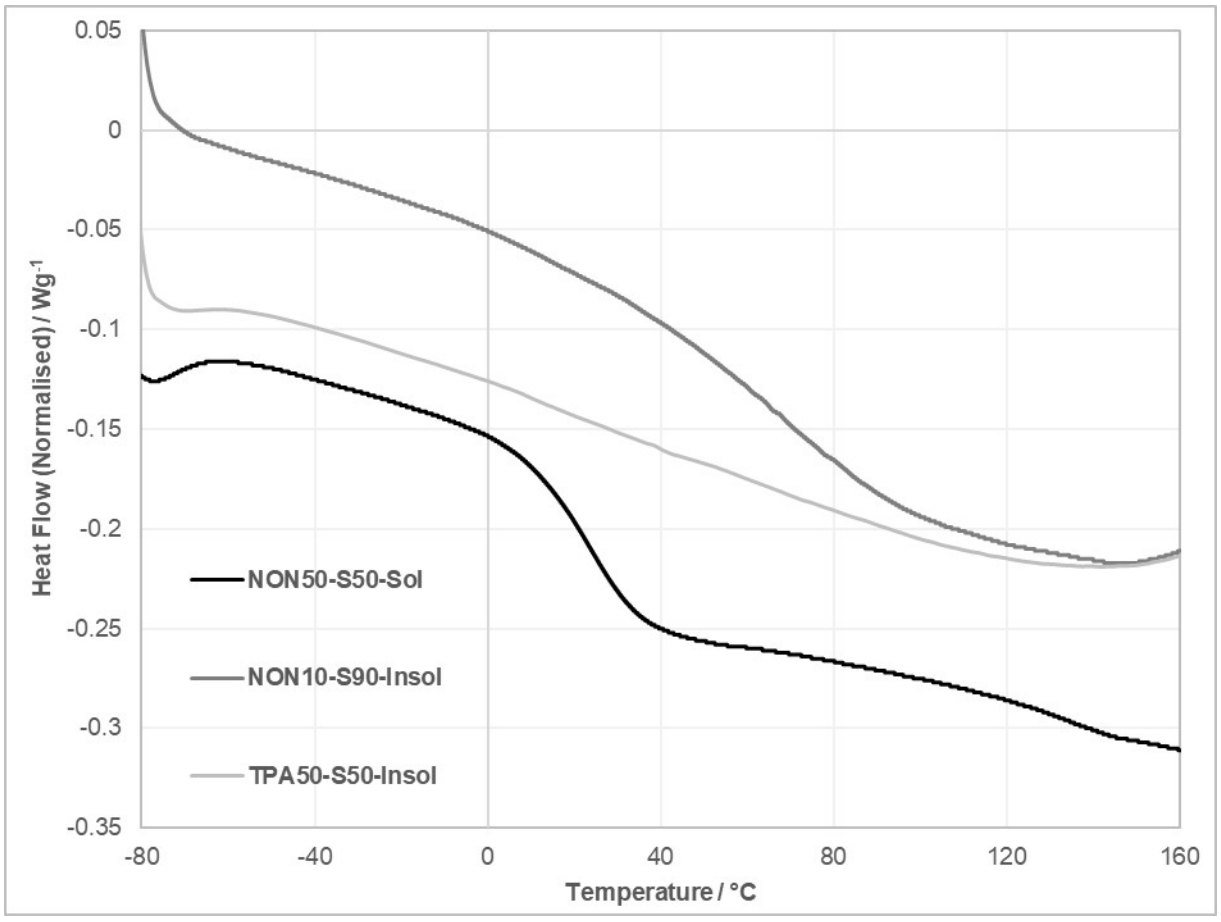

Figure S3: DSC thermograms of the second heating cycles for NON50-S50-Sol, NON10-S90-Insol, and TPA50-S50-Insol, showing a well-defined glass transition, a drawn-out glass transition, and no glass transition, respectively.

VI. FTIR Spectra

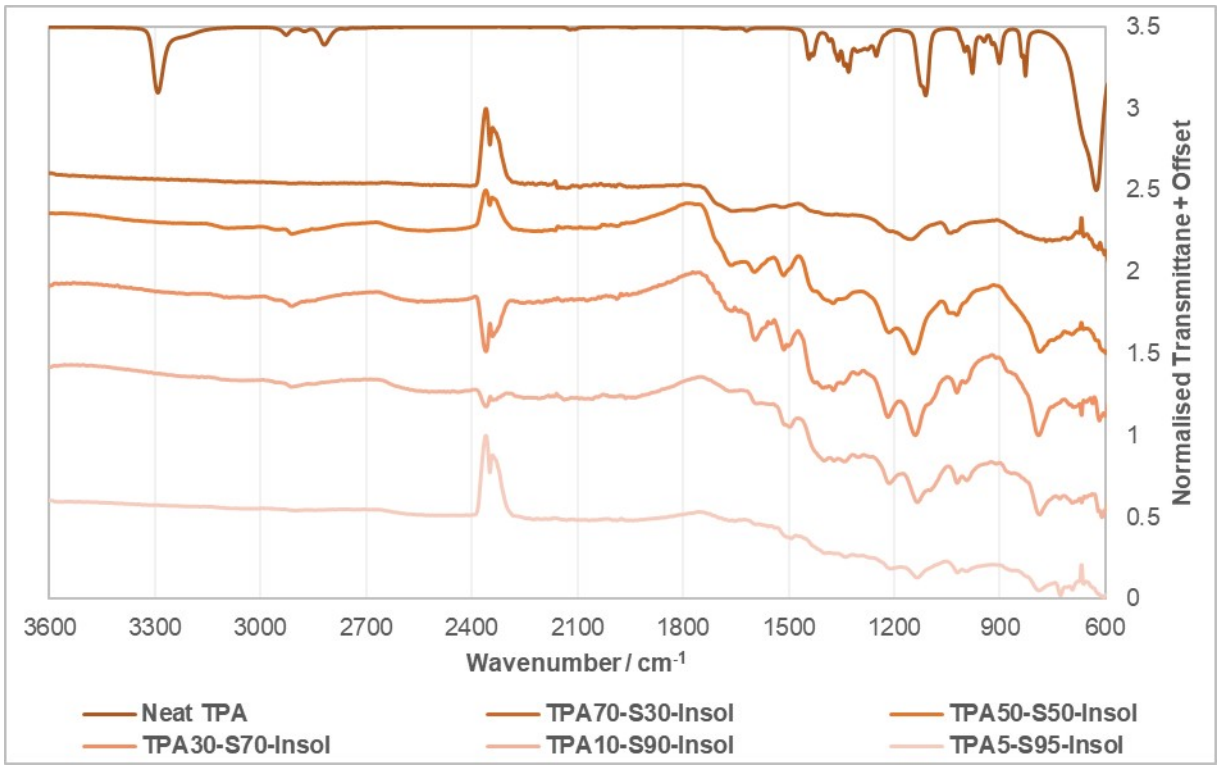

Figure S4: FTIR spectra for Insol polymers of TPA

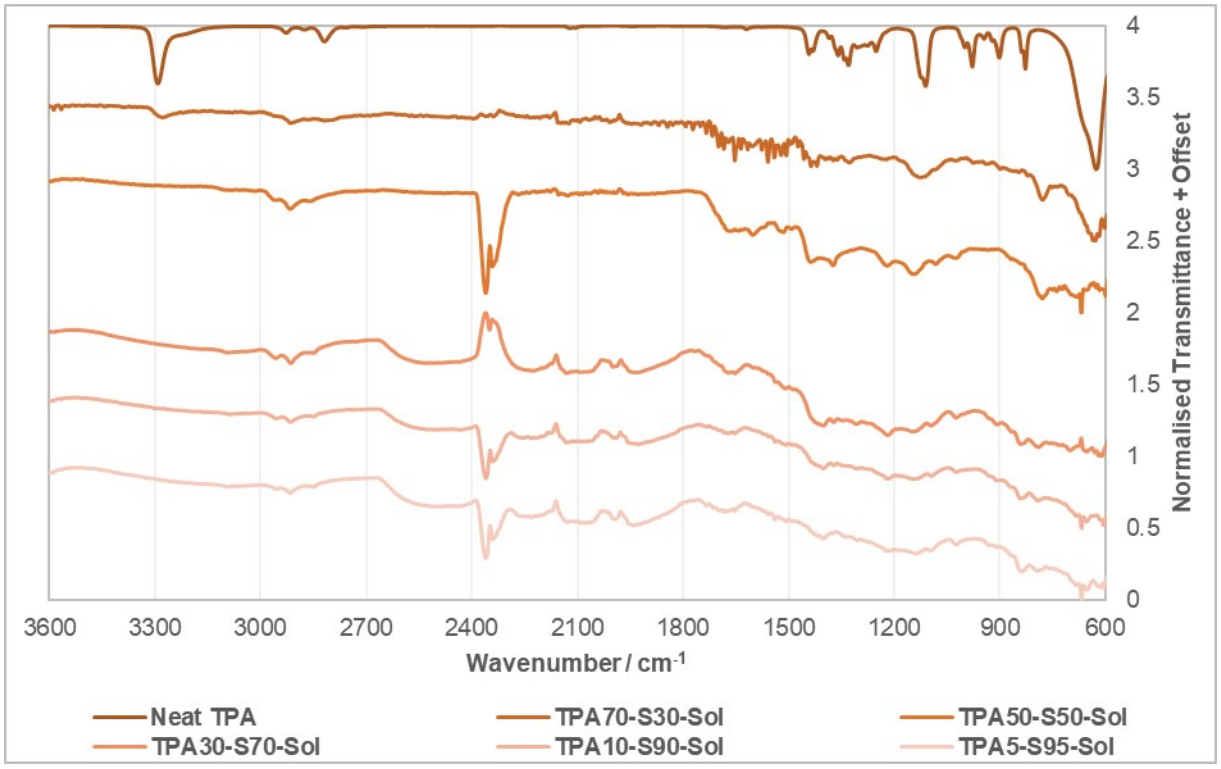

Figure S5: FTIR Spectra for Sol polymers of TPA

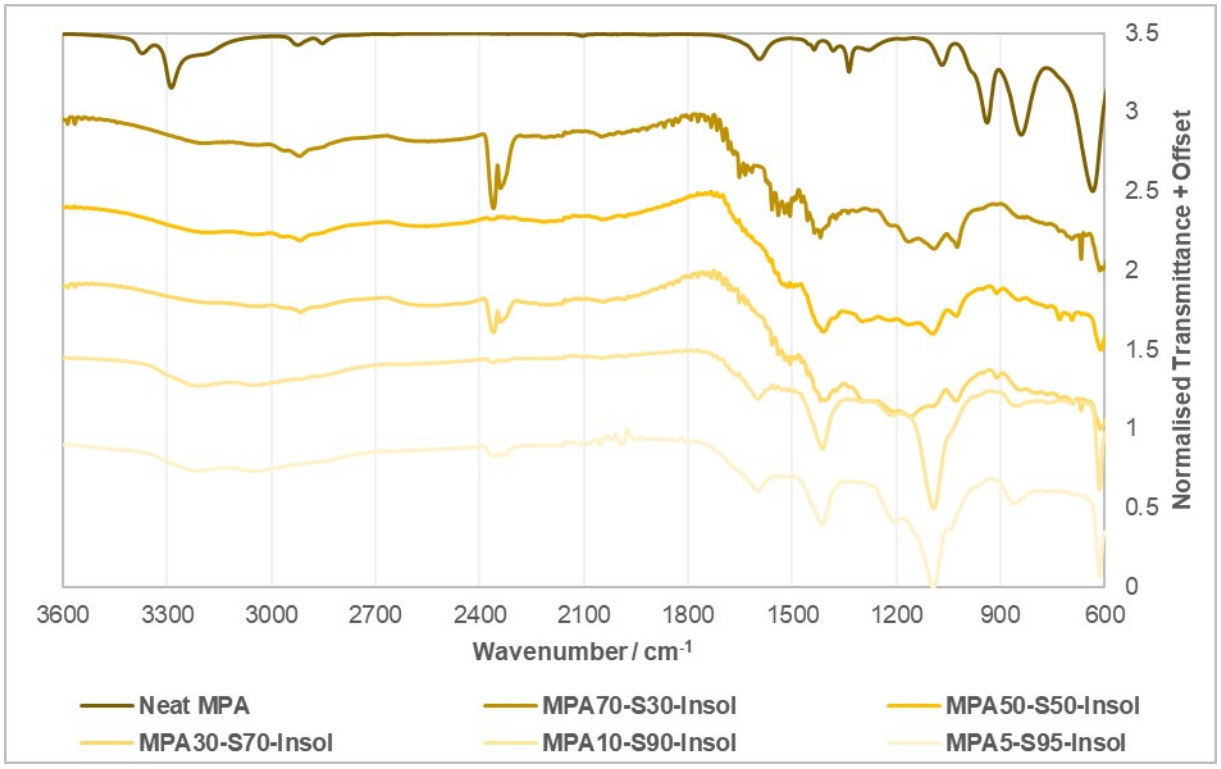

Figure S6: FTIR Spectra for Insol polymers of MPA

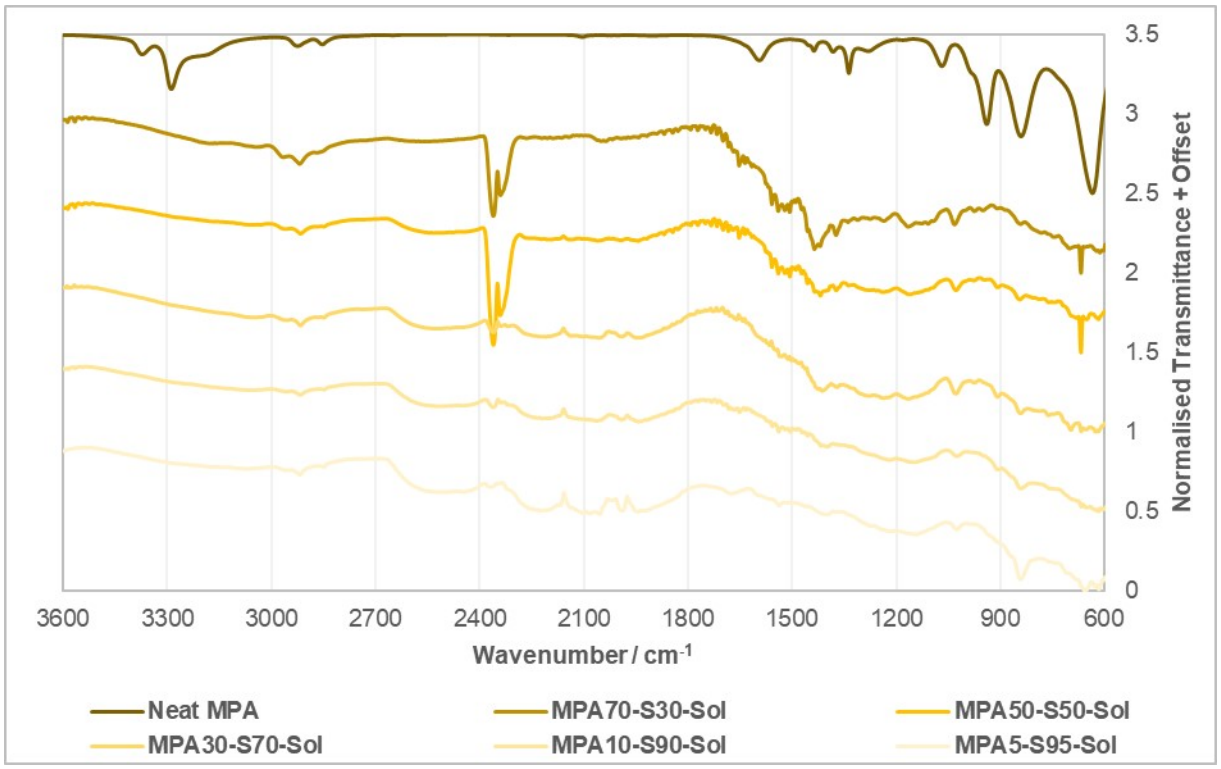

Figure S7: FTIR Spectra for Sol polymers of MPA

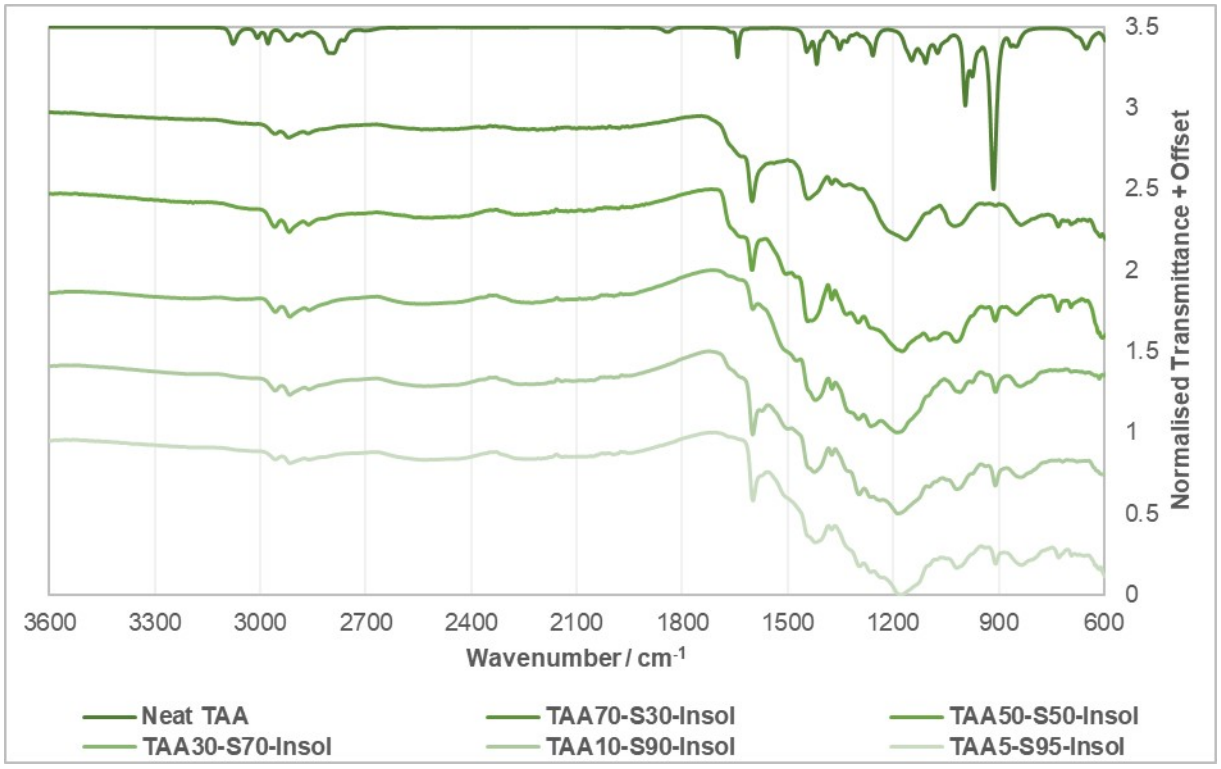

Figure S8: FTIR Spectra for Insol polymers of TAA

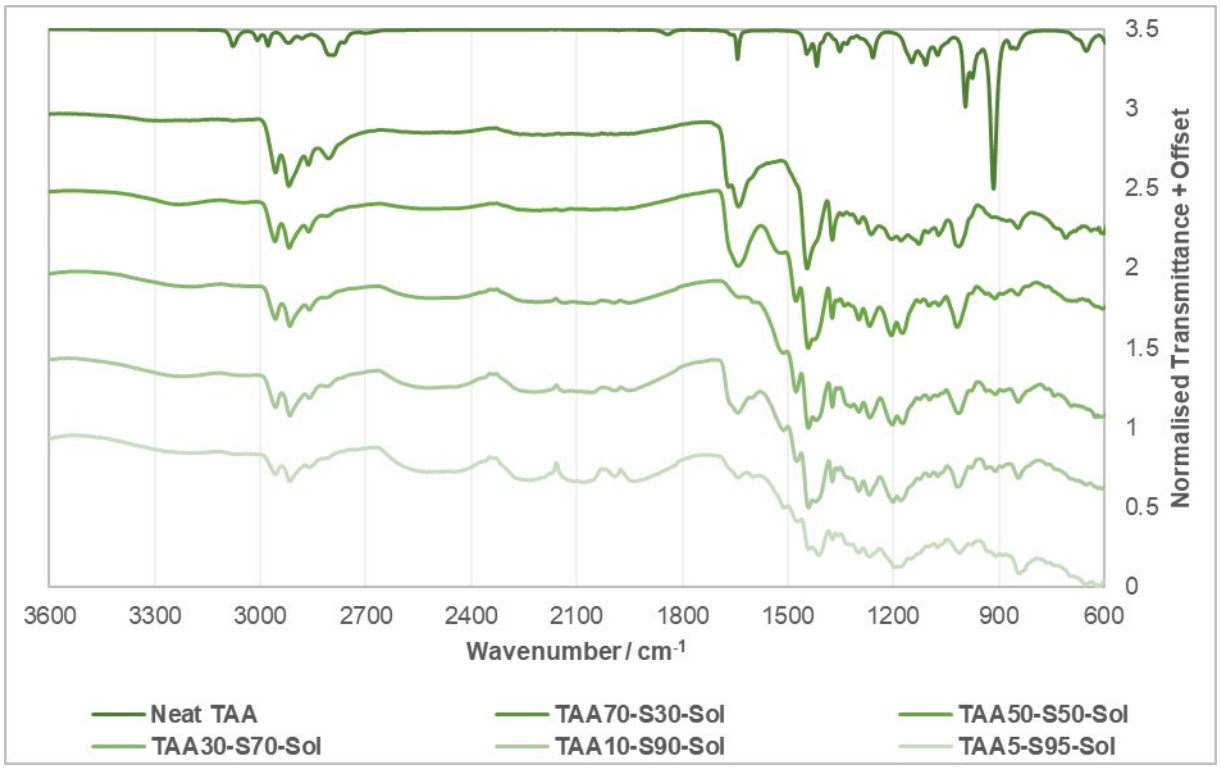

Figure S9: FTIR Spectra for Sol polymers of TAA

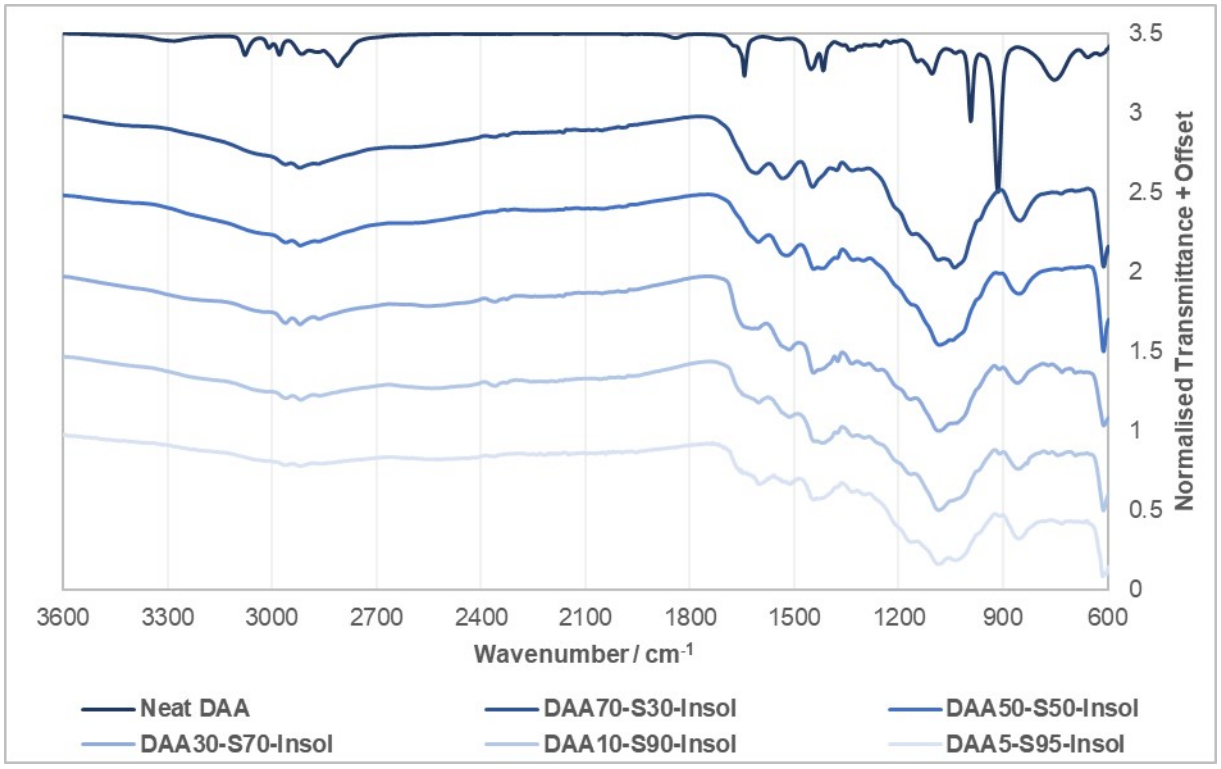

Figure S10: FTIR Spectra for Insol polymers of DAA

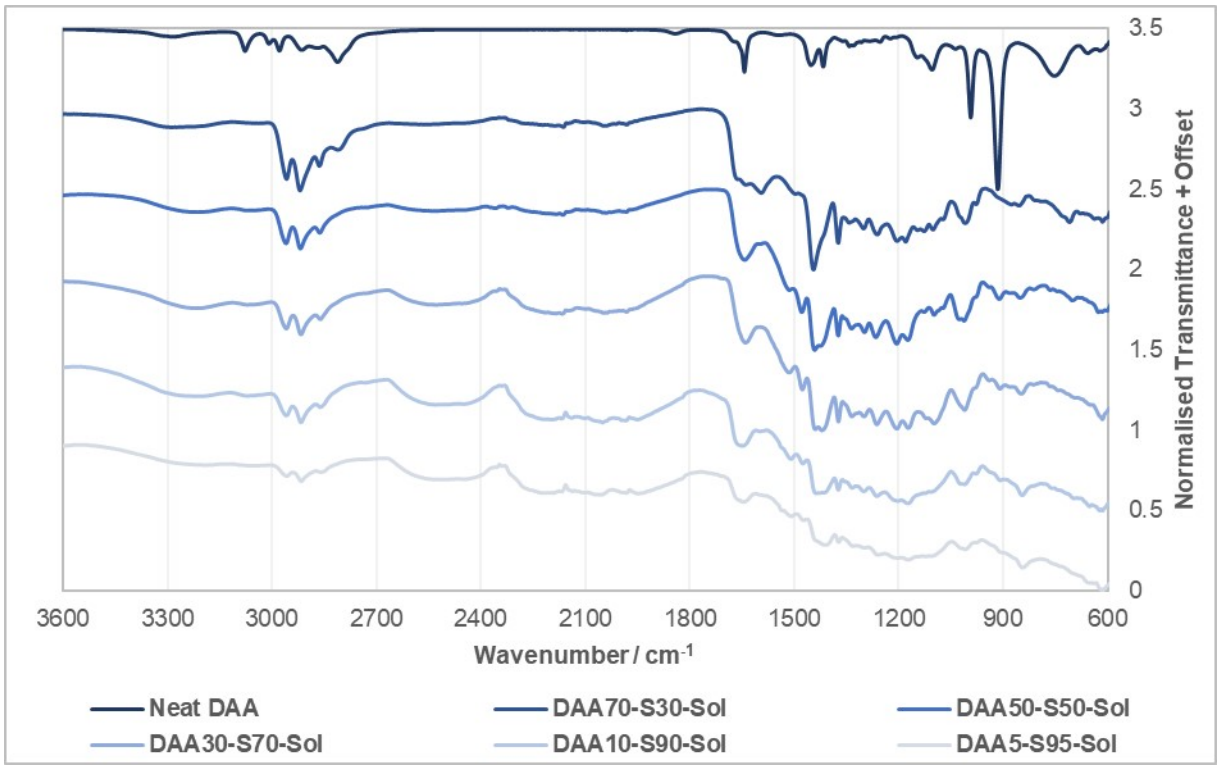

Figure S11: FTIR Spectra for Sol polymers of DAA

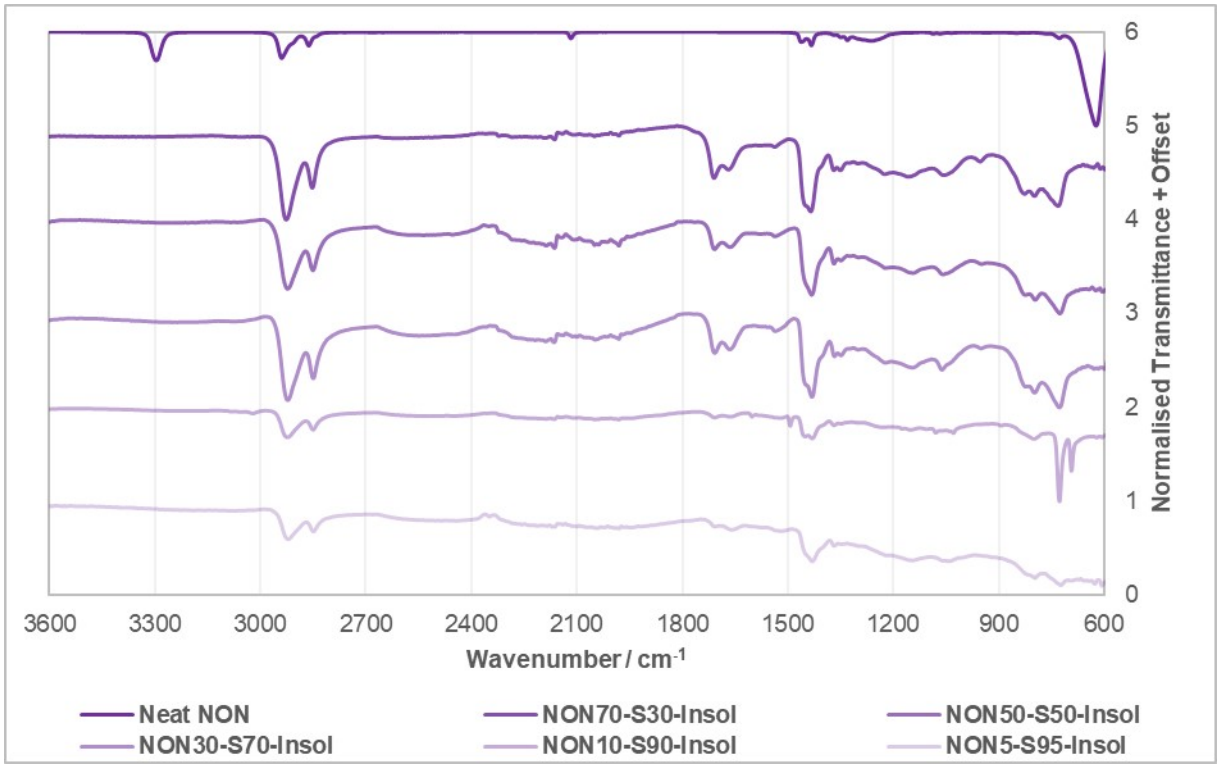

Figure S12: FTIR Spectra for Insol polymers of NON

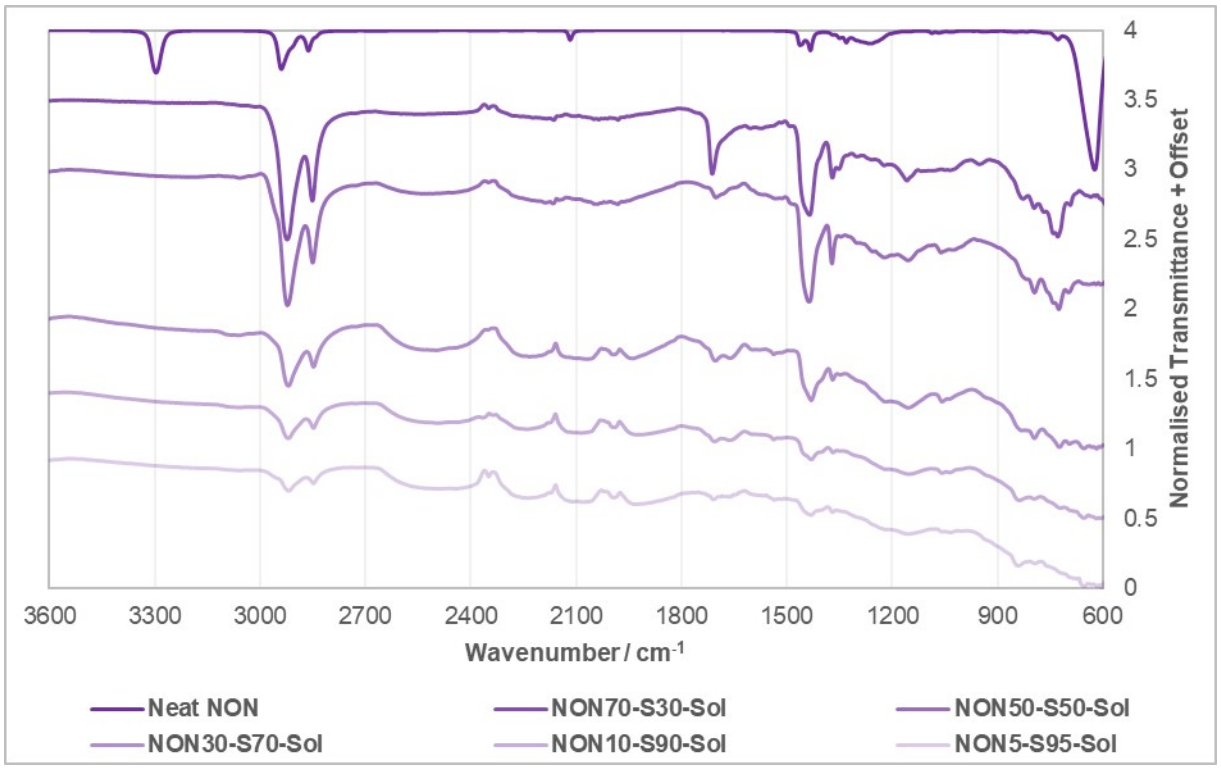

Figure S13: FTIR Spectra for Sol polymers of NON

VII. Computationally Predicted IR Data

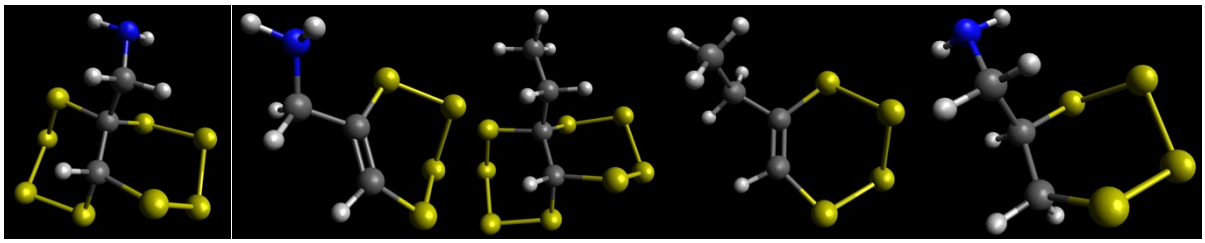

Figure S14: Geometry optimised structures for the models of the polymers. From left to right the identities are MPAfullreact (used in comparison to TPA and MPA polymers), MPApartreact (used in comparison to TPA and MPA polymers), NONfullreact (used in comparison to NON polymers), NONpartreact (used in comparison to NON polymers), TAAfullreact (used in comparison to TAA and DAA polymers). White atoms are hydrogen, grey atoms are carbon, yellow atoms are sulfur, and blue atoms are nitrogen.

Table S2: Calculated IR data for the models of the polymers, with particular modes of interest in bold

Model	Wavenumber / cm^{-1}	Assignment
MPAfullreact	653.659	1,2 - C-S asymmetric stretch, with skeletal vibrations
	692.846	1,1 - C-S asymmetric stretch, with skeletal vibrations
	718.928	1,1 - C-S symmetric stretch, with skeletal vibrations
	806.712	NH_2 vibration
	884.233	Carbon skeleton vibration with C-S asymmetric stretch
	936.638	C-C-C asymmetric stretch
	971.676	N-C-C-C asymmetric stretch
	1072.88	S_2C-H wag
	1100.89	N-C stretch
	1146.45	C-H and N-H wags
	1194.03	C-H and N-H wags
	1313.59	CH_2 wag
	1348.31	NH_2-CH_2 symmetric wag
	1417.62	CH_2 scissor
	1611.02	NH_2 scissor
	2966.67	CH_2 and C-H asymmetric stretch
	2972.10	CH_2 and C-H symmetric stretch
	3025.85	CH_2 asymmetric stretch
	3399.34	NH_2 symmetric stretch
	3482.25	NH_2 asymmetric stretch
MPApartreact	615.327	C-S stretch
	734.513	C-H, CH_2, NH_2 wags and rocks
	779.500	NH_2 vibration
	806.274	S-C=C-S asymmetric vibration
	913.527	C-C stretch with CH_2, NH_2 wags and rocks
	1026.36	C-N stretch
	1085.66	N-C-C asymmetric stretch
	1133.15	Skeletal vibration
	1235.64	C-H wag
	1280.10	C-H wag
	1353.66	CH_2 rock
	1441.48	CH_2 scissor
	1530.68	C=C stretch
	1599.81	NH_2 scissor
	2878.99	CH_2 asymmetric stretch
	2957.03	CH_2 asymmetric stretch
	3047.98	C-H stretch
	3414.73	NH_2 symmetric stretch
	3505.29	NH_2 asymmetric stretch
NONfullreact	643.226	1,2 - C-S asymmetric stretch, with skeletal vibrations
	685.627	1,1 - C-S asymmetric stretch, with skeletal vibrations

	724.624	C-S stretch with skeletal vibrations
	794.024	Carbon skeleton wag
	892.147	Carbon skeleton breathing
	953.569	C-C-C-C asymmetric stretch
	1032.35	CH_3-CH_2-CS2- asymmetric stretch of carbon bonds
	1065.63	CH wag with CH_3 rocking
	1074.46	Carbon skeletal vibration
	1082.87	Carbon skeletal vibration
	1183.42	CH wag
	1266.29	CH_2 rock
	1308.42	CH_2 rock
	1363.66	CH_3 vibration
	1419.88	CH_2 scissor
	1443.19	CH_3 vibration
	1452.41	CH_3 scissor
	2953.30	CH_2 symmetric stretch
	2972.56	All CH bonds breathing
	2976.19	CH_3 breathing
	3013.59	CH vibrations
	3044.29	CH_3 asymmetric stretch
	3051.51	CH vibrations
NONpartreact	603.739	C-S stretch
	735.193	C-S stretch with carbon skeleton vibrations
	753.278	Carbon skeleton rocking
	813.427	S-C=C-S asymmetric stretch
	907.745	C-C-C symmetric stretch with C-S stretch
	1025.29	C-C-C asymmetric stretch with C-S stretch
	1053.10	C=C stretch with carbon skeleton vibrations
	1090.41	C-C-C=C central bond stretch
	1222.32	C=C stretch with carbon skeleton vibrations
	1270.10	C-S stretch with carbon skeleton vibrations
	1291.48	CH_2 rock
	1358.33	CH_3 vibration
	1429.13	CH_2 scissor
	1444.29	CH_3 vibration
	1455.89	CH_3 scissor
	1543.23	C=C stretch
	2942.55	CH_2 symmetric stretch
	2966.23	CH_3 breathing
	2988.42	CH_2 asymmetric stretch
	3037.72	CH_3 asymmetric stretch
	3042.52	CH_3 asymmetric stretch
	3053.32	C=C-H stretch
TAAfullreact	655.125	C-S stretch
	791.242	C-S stretch with carbon skeleton + NH_2 vibrations
	839.355	Carbon skeleton rocking + NH_2 vibrations
	871.885	Carbon skeleton rocking + NH_2 vibrations
	956.764	S-C-C-S stretch
	1004.36	C-C-C asymmetric stretch
	1075.13	N-H stretch
	1107.25	Carbon skeleton stretches + NH_2 vibrations
	1163.14	Carbon skeleton stretches
	1184.16	C-H wags with C-S stretch
	1240.40	Carbon skeleton wag + NH_2 wag
	1260.50	C-H wags with C-S stretch
	1325.13	C-H and N-H wags
	1346.23	NH_2-CH_2 symmetric wag
	1381.29	S-CH_2 scissoring
	1430.28	N-CH_2 scissoring
	1612.34	NH_2 scissoring
	2931.91	C-H vibrations
	2949.52	CH_2 symmetric stretches
	2960.86	C-H breathing
	3012.98	CH_2 asymmetric stretches
	3022.48	S-CH_2 asymmetric stretch
	3388.41	NH_2 symmetric stretch
	3466.67	NH_2 asymmetric stretch

VIII. CHNS and XRF

Table S3: Unreliable combustion microanalysis data for Sol and Insol products of TPA, TAA, and NON polymers

Polymer Name	Expected				Combustion Microanalyses			
	%C	%H	%N	%S	%C	%H	%N	%S
TPA70-S30-sol	57.69	4.84	7.48	30.00	62.55	5.49	7.73	23.44
TPA70-S30-insol					46.30	3.37	5.38	36.30
TPA50-S50-sol	41.21	3.46	5.34	50.00	58.26	5.19	6.95	28.90
TPA50-S50-insol					41.18	2.85	4.93	45.16
TPA30-S70-sol	24.72	2.08	3.20	70.00	15.28	1.59	1.28	82.16
TPA30-S70-insol					37.53	2.69	4.37	55.26
TPA10-S90-sol	8.24	0.69	1.07	90.00	4.44	0.80	0.00	97.30
TPA10-S90-insol					38.80	2.16	4.35	53.42
TPA05-S95-sol	4.12	0.35	0.53	95.00	3.97	0.70	0.00	97.45
TPA05-S95-insol					39.27	2.21	4.21	53.67
TAA70-S30-sol	55.14	7.71	7.15	30.00	53.83	6.76	6.41	32.01
TAA70-S30-insol					46.30	3.37	5.38	36.30
TAA50-S50-sol	39.39	5.51	5.11	50.00	45.78	3.83	5.05	43.08
TAA50-S50-insol					41.18	2.85	4.93	45.16
TAA30-S70-sol	23.63	3.31	3.06	70.00	24.16	2.80	2.75	69.77
TAA30-S70-insol					37.53	2.69	4.37	55.26
TAA10-S90-sol	7.88	1.10	1.02	90.00	11.29	1.55	0.08	88.79
TAA10-S90-insol					38.80	2.16	4.35	53.42
TAA05-S95-sol	3.94	0.55	0.51	95.00	7.07	1.24	0.38	93.91
TAA05-S95-insol					39.27	2.21	4.21	53.67
NON30-S70-sol	26.98	3.02	0.00	70.00	8.19	1.34	0.00	94.02
NON30-S70-insol					39.43	3.93	0.00	55.78
NON10-S90-sol	8.99	1.01	0.00	90.00	3.27	0.70	0.00	99.20
NON10-S90-insol					44.11	4.45	0.00	50.49

For the following results, the polymers were synthesized via bulk polymerisation, as described in Section II.D. of the supporting information with a few modifications. Briefly, sulfur was melted and thermally equilibrated over ten minutes at 135 °C. then, DVB (weighed by difference) was added to the vial, which was then immediately sealed with a septum and air balloon, minimising crosslinker evaporation whilst allowing pressure regulation. The reactions were left overnight with 800 rpm stirring.

Table S4: Comparison of combustion microanalysis and XRF data for some standard DVB polymers

Polymer	Reactant masses / g	Yield	Expected			Combustion Microanalyses			XRF
			%C	%H	%S	%C	%H	%S	%S
DVB70-S30	DVB: 6.9785 g S_8: 3.0062 g	9.4947 g 95.08 %	63.05	5.29	31.67	62.80	5.37	31.39	34.82
DVB50-S50-A	DVB: 4.9885 g S_8: 5.0064 g	9.6995 g 97.05 %	44.64	3.75	51.61	44.16	3.75	51.81	62.42
DVB50-S50-B	DVB: 4.9888 g S_8: 5.0058 g	9.7355 g 97.40 %	44.82	3.76	51.42	43.98	3.74	51.82	60.62
DVB30-S70	DVB: 2.9944 g S_8: 7.0075 g	9.8924 g 98.91 %	26.91	2.26	70.83	25.96	2.33	72.13	85.39

Expected CHNS values were calculated by assuming that all losses to the yield were the result of crosslinker evaporation. Table S4 shows that combustion microanalysis can be remarkably accurate when the polymerisation is carefully controlled, and the volatilisation of crosslinker is accounted for. The XRF over-estimates the quantity of sulfur, and it is found that this is because of the one hour exposure time used in these initial XRF experiments. Later experiments with very short exposure times underestimated the amount of sulfur, and the longer the exposure time was, the more the sulfur content was less underestimated and became more over estimated. This is presumed to be due to the carbon content being burned off by the X-rays. Great effort was made to find a method of XRF analysis that produced trustworthy results, but these efforts were ultimately fruitless. No suitable baseline could be created for the measurements which could've been due to a combination of matrix effects (which cannot easily be taken into account in the largely unstudied structures of inverse vulcanised polymers), and the lack of stability in the baseline between measurements. Numerous other issues were encountered, such as inconsistent and complex shaped calibration curves which could've been a result of changing sample density. For high density samples, the XRF response tends to come from a hemisphere of the sample under the irradiation point, but in higher density samples, the X-rays penetrate deeper in and give a response from deeper in the sample, resulting in a tear drop shaped response zone. Since sulfur polymers vary in density as their sulfur loading changes, it was believed that the response zone was changing shape from a hemi-sphere for high density samples, to a tear-drop at lower density samples, and that this could have resulted in a change in the signal response with sulfur loading, however attempts to take this into account were not successful in yielding sensible calibration curves, meaning that either this hypothesis is untrue, or there are more unaccounted for effects.

IX. NMR of the Degradation Products

Firstly, approximately 100 mg of polymer was added to an oven dried 14 mL glass vial containing a PTFE stirrer, all of which was sealed with a septum and purged with nitrogen for a few minutes. Afterward 5 mL of 1 M $LiAlH_4$ in THF was injected into the vial, and the reaction was left stirring overnight with a nitrogen balloon affixed. The next day it was noted that there was still remaining solid in the reaction solution, indicating that the $LiAlH_4$ the reaction had not gone to completion in terms of degrading the polymer structure. The reaction solution was quenched by the dropwise addition of deionised water until addition of more water caused no further fizzing, at which point 1 M HCl in deionised water was added to make the reaction solution up to 10 mL. During the quench, vigorous fizzing was noted, indicating that there was plentiful $LiAlH_4$ remaining. The reaction mixture was transferred into a 20 mL vial, where in the aqueous phase was extracted three times with EtOAc. The EtOAc, usually clear yellow, clear orange, or clear brown in colour, was washed with brine and dried over $MgSO_4$, before it was evaporated to dryness, leaving a solid residue. The residue was analysed by ^{1}H NMR, ^{13}C NMR, ^{13}C DEPT135 NMR, ^{1}H ^{1}H COSY NMR, and ^{1}H ^{13}C HSQC NMR. This process was performed on the Sol and Insol products of TPA50-S50, TAA50-S50, NON50-S50, MPPA50-S50, and DAA50-S50, though it is important to note that the EtOAc extracts from the TPA50-S50-Insol and NNON50-S50-Insol were clear and colourless, and yielded no residue when evaporated to dryness.

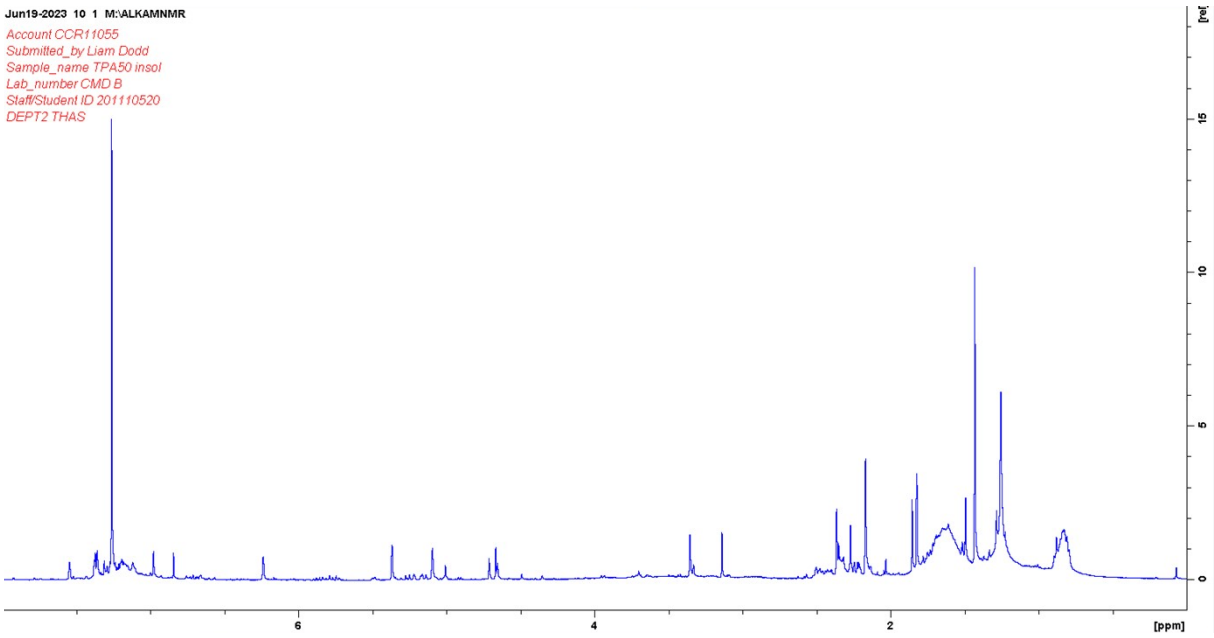

Figure S15: The ^{1}H NMR spectrum of the degradation products of TPA50-S50-Sol. Note that in the figure the title suggests the sample is that of an Insol. This is a mistake in the naming, but sample is indeed TPA50-S50-Sol.

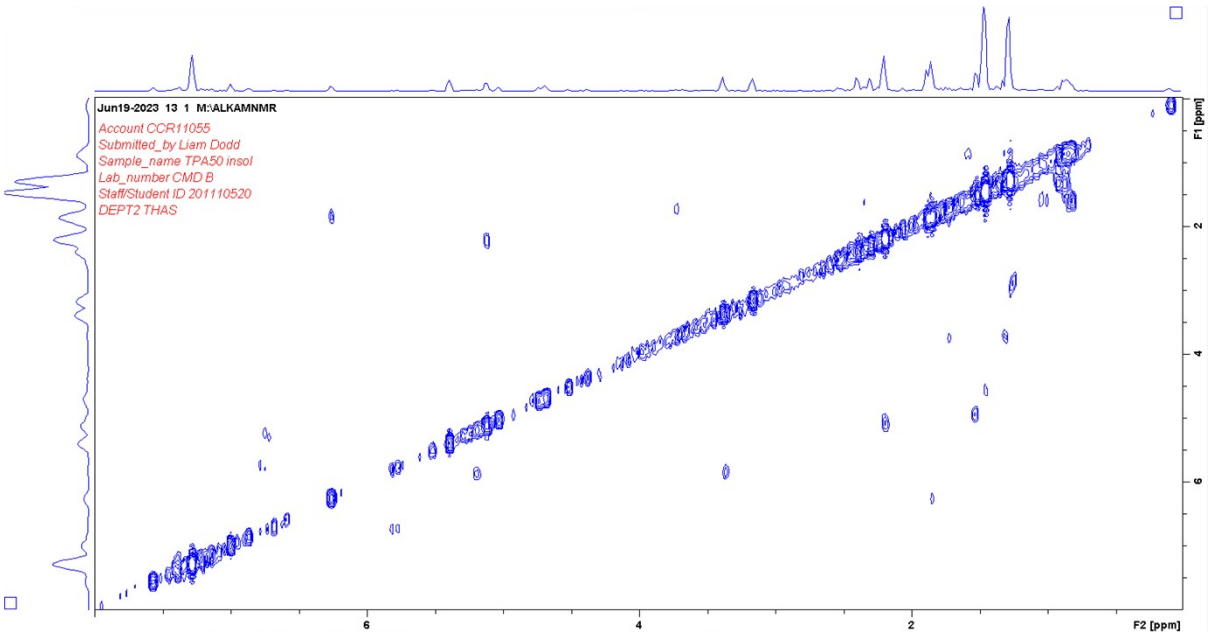

Figure S16: The ^{1}H ^{1}H COSY NMR spectrum of the degradation products of TPA50-S50-Sol. Note that in the figure the title suggests the sample is that of an Insol. This is a mistake in the naming, but sample is indeed TPA50-S50-Sol.

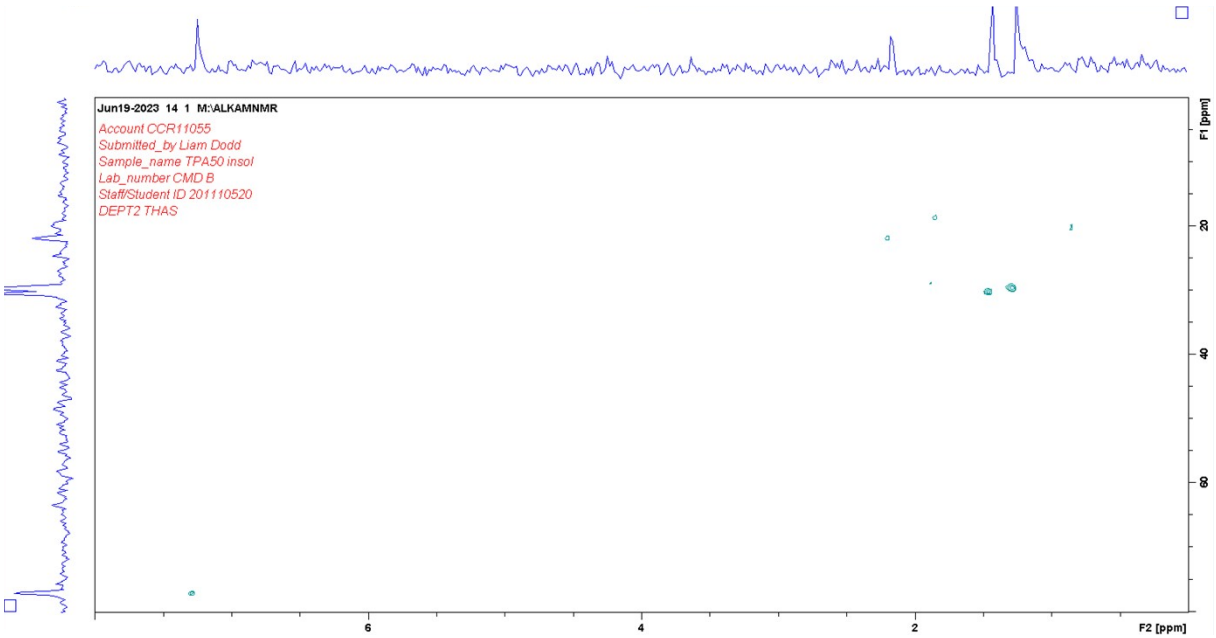

Figure S17: The ^{1}H ^{13}C HSQC NMR spectrum of the degradation products of TPA50-S50-Sol. Note that in the figure the title suggests the sample is that of an Insol. This is a mistake in the naming, but sample is indeed TPA50-S50-Sol.

Figure S15 contains numerous broad peaks over wide chemical shift ranges, suggesting that the degradation products are oligomeric in nature, rather than clean cut monomer units. Figure S15 does however provide some insights. First of all, though they are of low integration, there appears to aromatic hydrogens between 7.5 ppm and 6.5 ppm. These have been attributed to thiophenes, as the

signals seem to be for the most party singlets, which would be explained by the formation of a thiophene structure. However, thiophene resonances would be expected below 7 ppm, so it also proposed that there is some formation of benzene rings and thiophenol rings, which would explain the dense multiplet above 7 ppm, as well as the peaks as high as 7.5 ppm. Figure S16 shows that the thiophene resonances are not coupled to the benzene resonances, supporting the conclusion that these resonances belong to separate types of fragment. Figure S16 also shows that there is coupling between the supposed thiophene resonance at 6.24 and the resonance at 1.85 which could be an alkyl fragment bound to the thiophene ring. The peak at 3.35 ppm is dubiously attributed to a thiophenol thiol, because it occurs in the expected range, but is not broad as would be expected. Importantly, these aromatic peaks are much weaker than the alkyl region, which may suggest that these aromatic fragments are by-products rather than the predominant species. Another minority by-product appears to be alkenes, as there are resonances in the region of 5.5 to 5 ppm, which is in agreement with the results of the FTIR spectroscopy that the alkynes may react to form alkenes first, before reacting onward. Below 2.5 ppm is where the majority of the signals are, but it is too complex to analyse in detail. There are several broad peaks in this range which could be attributed to the thiol hydrogens that would be expected of this degradation product. There seems to be numerous alkyl resonances scattered throughout the region, which Figure S16 shows are intercoupled in a complex manner, again suggesting an oligomeric structure for the degradation product. The ^{13}C NMR and DEPT135 ^{13}C NMR failed to give any signals, despite being placed on a long NMR experiment to enhance their signal to noise ratios. Strangely, Figure S17 shows that the ^{1}H ^{13}C HSQC NMR did manage to acquire ^{13}C signals, but overall Figure S17 does not provide much diagnostic information. Figure S18 shows potential ways that thiophenes, benzenes and thiophenols could form.

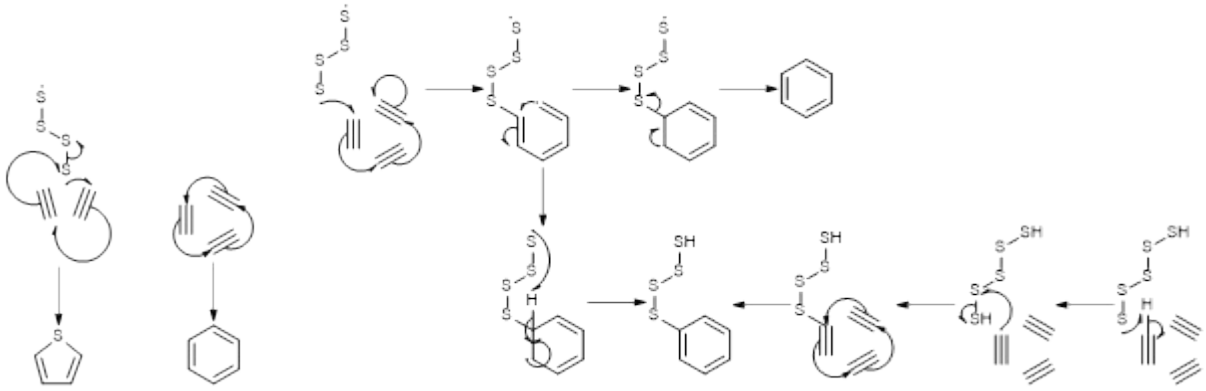

Figure S18: Potential mechanisms for the formation of the aromatic by-products. R groups have been omitted for clarity.

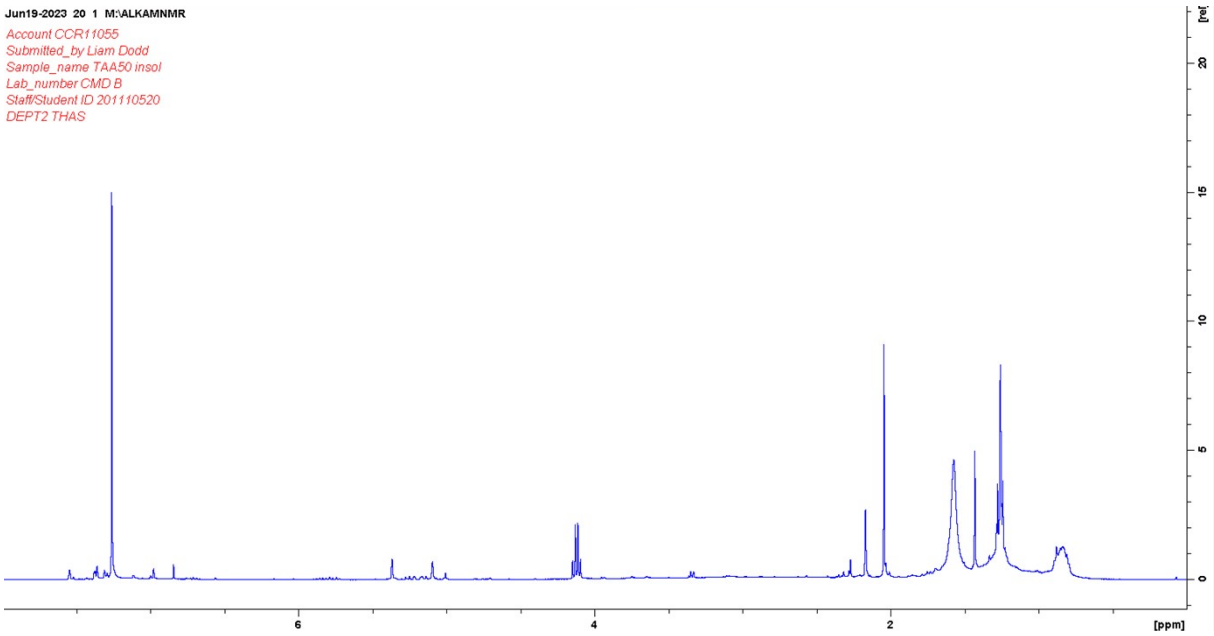

Figure S19: The ^{1}H NMR spectrum of the degradation products of TAA50-S50-Insol.

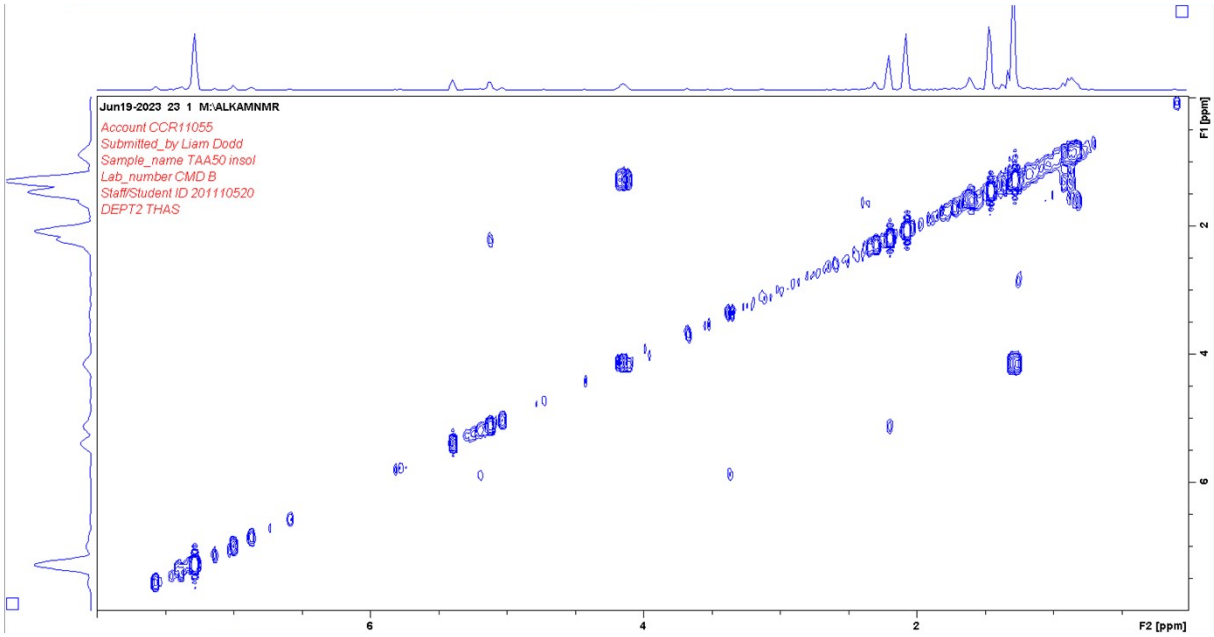

Figure S20: The ^{1}H ^{1}H COSY NMR spectrum of the degradation products of TAA50-S50-Insol.

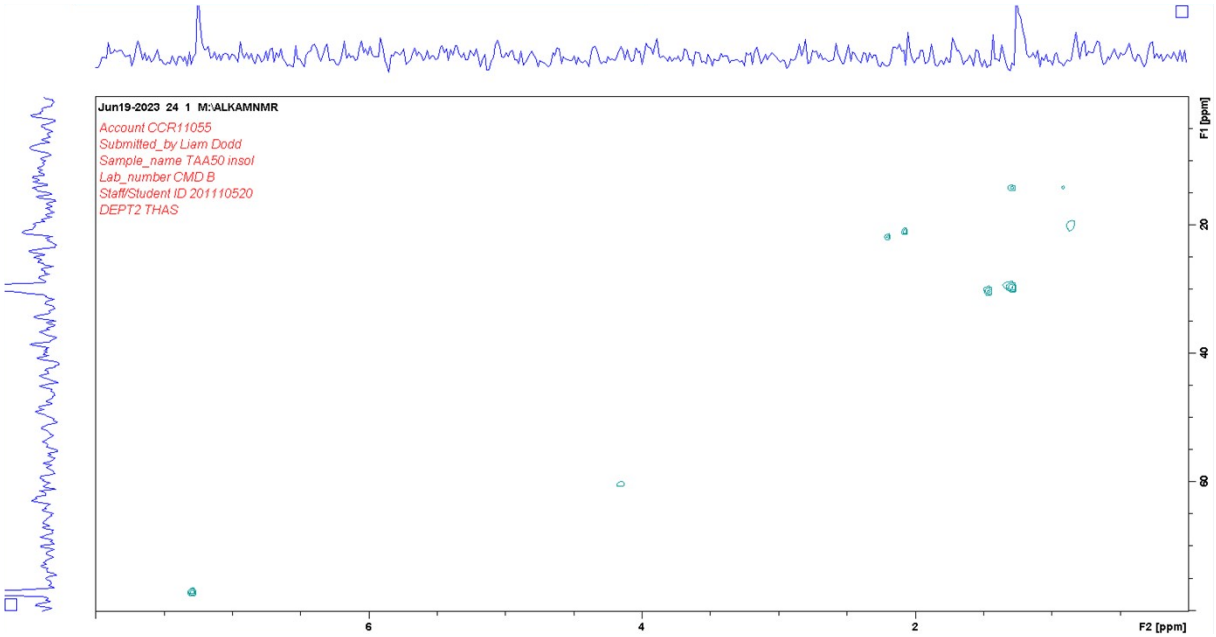

Figure S21: The ^{1}H ^{13}C HSQC NMR spectrum of the degradation products of TAA50-S50-Insol.

Figure S19 shows that much like TPA50-S50-Sol, TAA50-S50-Insol shows some aromatic signals, many of them matching closely to those of TPA50-S50-Sol, with the exception of the broad peak at about 7.25 ppm that appears in the TPA50-S50-Sol spectrum, but not in the TAA50-S50-Insol spectrum, suggesting that TAA50-S50-Insol cannot form all the aromatic species that TPA50-S50-Sol can. Based on the assignments from the TPA50-S50-Sol spectrum, it may be that TAA50-S50-Sol cannot form benzenes or thiophenols but still can form thiophenes. The peaks that appear in Figure S15 between 4.75 ppm and 3.5 ppm do not appear in Figure S19 though it is hard to assign these peaks with any certainty. This does point to the fact that TAA50-S50-Insol may have fewer reaction pathways in its formation as compared to TPA50-S50-Sol. This might be expected since the alkyne functional group adds another pi bond in comparison to the alkene group, and TPA derived polymers could be expected to be more complex than TAA derived polymers. What else supports this conclusion in that for TAA50-S50-Insol, the lower chemical shift region of the spectrum is notably less dense with signals than the analogous region in the TPA50-S50-Sol region. That being said, several signals in this region directly match between the two polymers, namely those a t 0.85 ppm, 1.25 ppm and 1.45 ppm. This suggests that there is a significant degree of similarity between the polymers which may imply that TPA can react via similar pathways to TAA, thus generating somewhat similar polymers. This may also imply that alkyne bonds can react in a similar way to alkene bonds, thus producing products that are similar; in other words, this may be evidence that alkynes do react as expected in inverse vulcanisation. Note that Figure S19 does show signals for ethyl acetate. Once again, the ^{13}C NMR and DEPT135 ^{13}C NMR did not yield any signals through the noise for TAA50-S50-Insol, though the ^{1}H ^{13}C HSQC did manage to produce a very weak ^{13}C NMR spectrum, though the HSQC itself is not of particular utility in understanding the polymer structure.

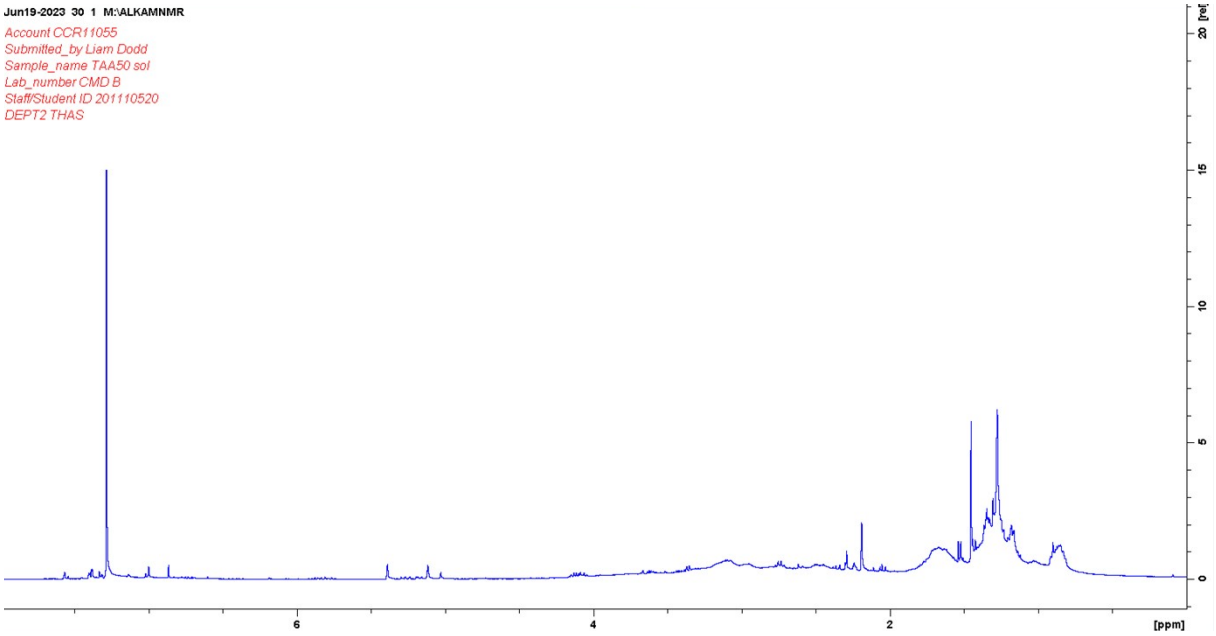

Figure S22: The ^{1}H NMR spectrum of the degradation products of TAA50-S50-Sol.

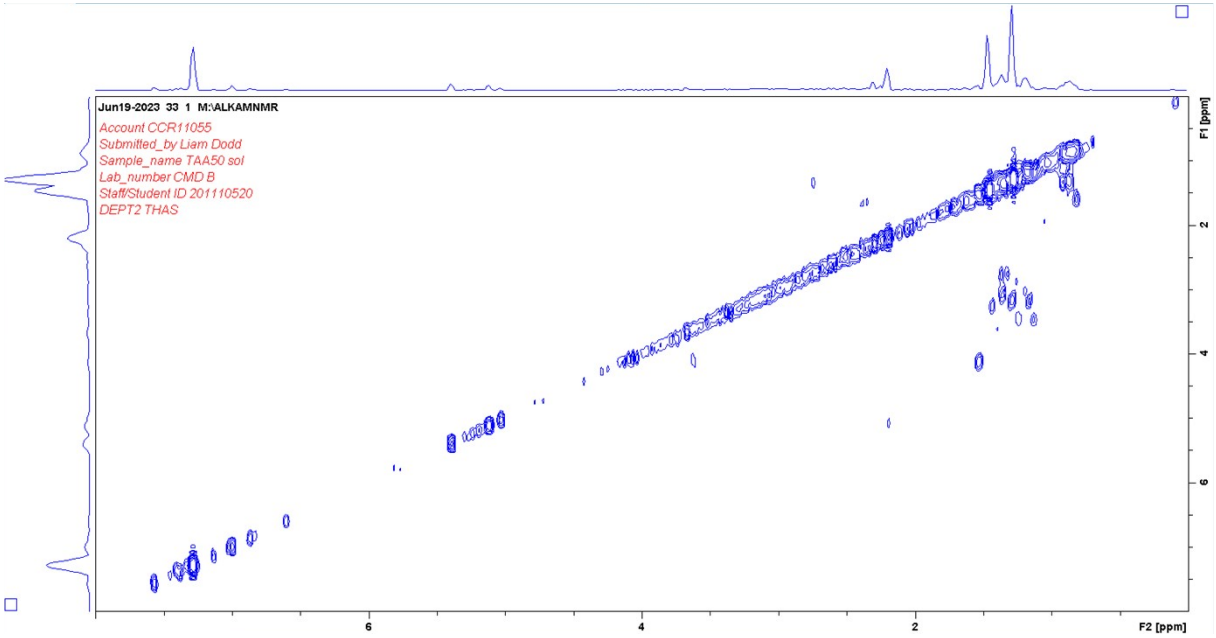

Figure S23: The ^{1}H ^{1}H COSY NMR spectrum of the degradation products of TAA50-S50-Sol.

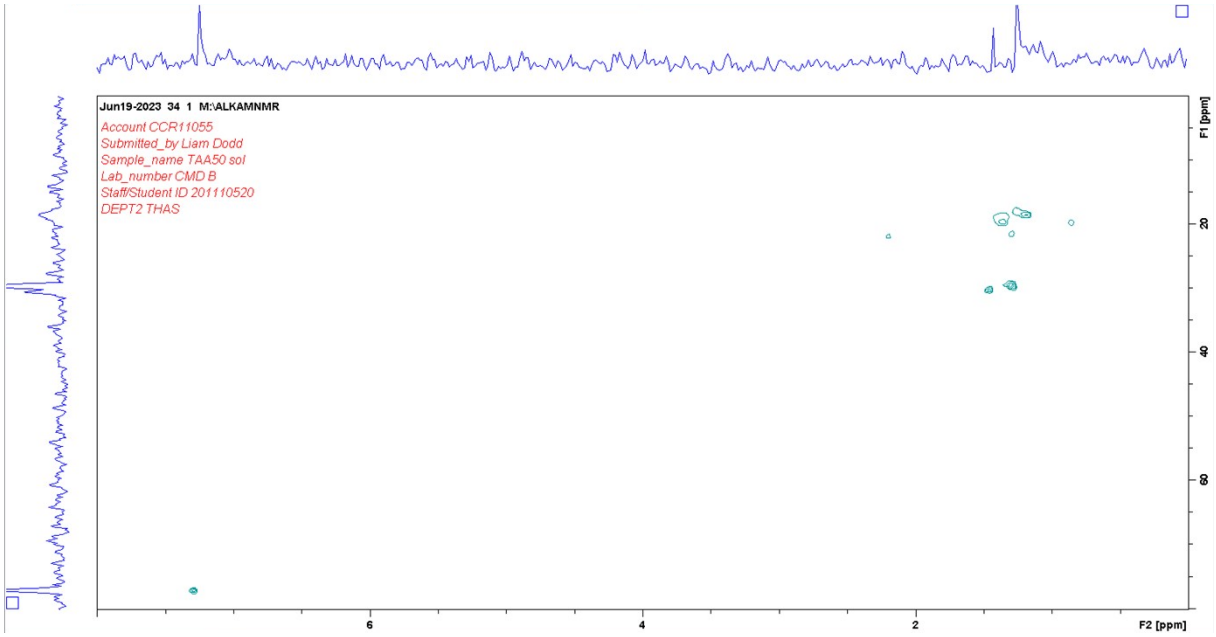

Figure S24: The ^{1}H ^{13}C HSQC NMR spectrum of the degradation products of TAA50-S50-Sol.

Observing Figure S22, many of the same conclusions that were drawn from TPA50-S50-Sol and TAA50-S50-Insol can be made about TAA50-S50-Sol. One thing that is clear, is that the NMR spectra of TAA50-S50-Sol is more complex than the spectra of TAA50-S50-Insol. In addition to this, TAA50-S50-Sol shows some broad peaks in its spectra, which are absent int the spectrum of TAA50-S50-Insol, but have analogous peaks in the spectra of TPA50-S50-Sol. This implies that the Sol products have a tendency to display more broad peaks, which points toward the conclusion that the Sol products are less well defined than the Insol products, and have more by-product fragments in their structure. Once again, the ^{13}C NMR and DEPT135 ^{13}C NMR did not yield any signals through the noise for TAA50-S50-Sol, though the ^{1}H ^{13}C HSQC did manage to produce a very weak ^{13}C NMR spectrum, though the HSQC itself is not of particular utility in understanding the polymer structure.

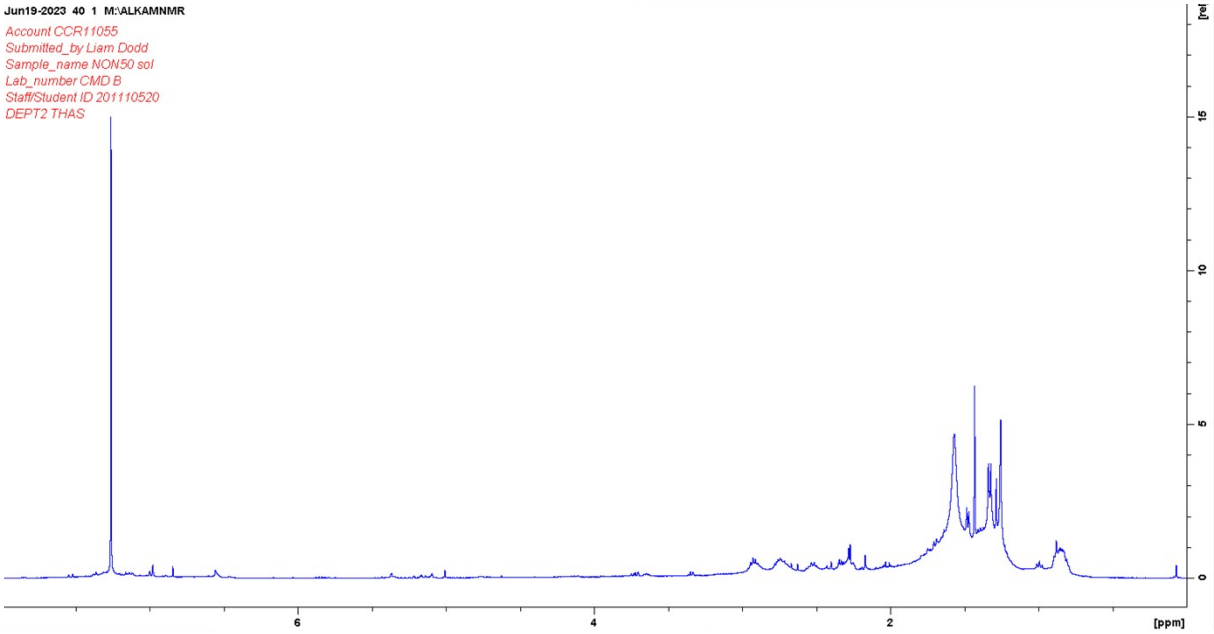

Figure S25: The ^{1}H NMR spectrum of the degradation products of NON50-S50-Sol.

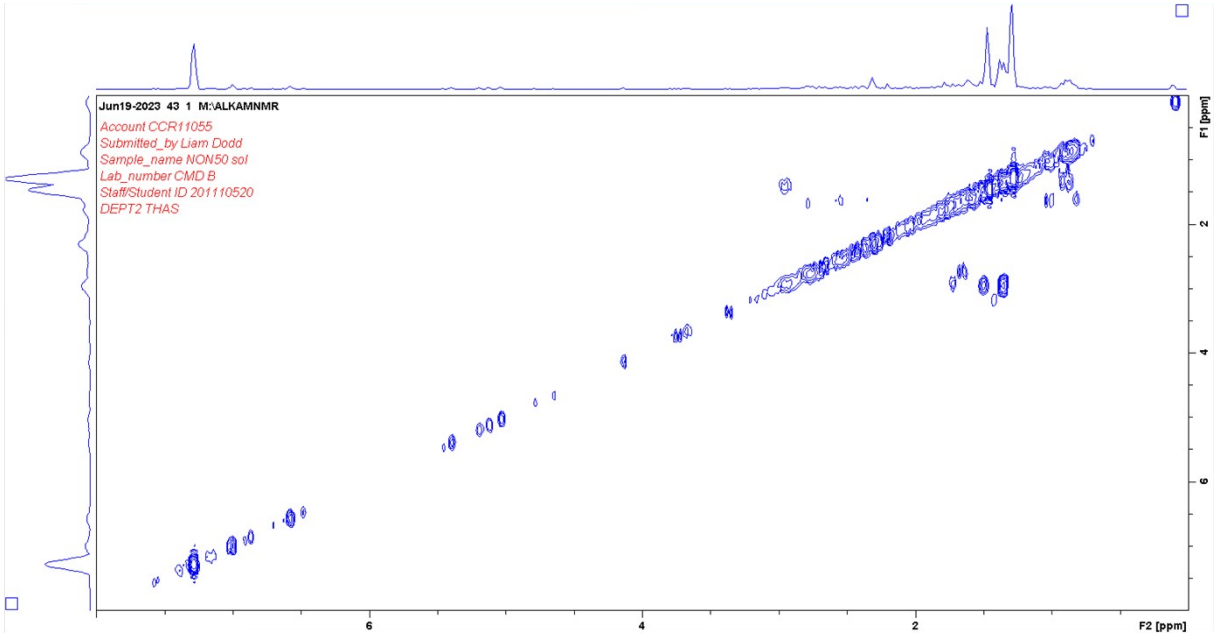

Figure S26: The ^{1}H ^{1}H COSY NMR spectrum of the degradation products of NON50-S50-Sol.

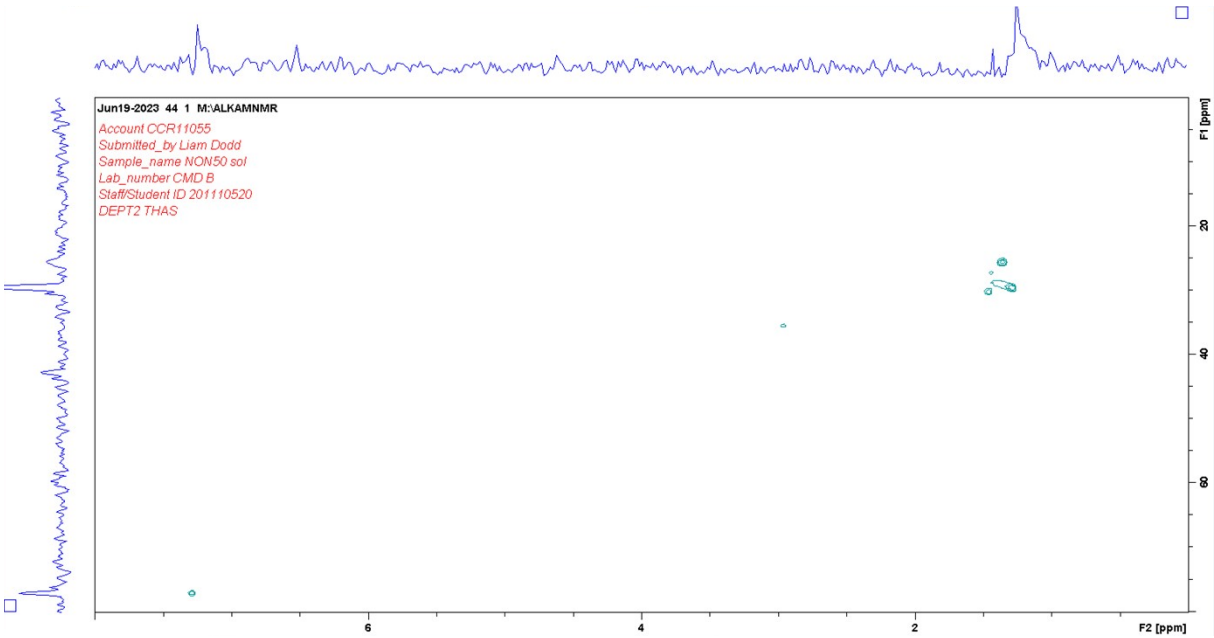

Figure S27: The ^{1}H ^{13}C HSQC NMR spectrum of the degradation products of NON50-S50-Sol.

Figure S25 shows that the ^{1}H NMR spectrum for NON50-S50-Sol is notably different to those of TAA or TPA polymers, likely due to the significant structural dissimilarity, and the higher predominance of aliphatic protons (NON has five CH_2 groups, in three separate environments, whereas TAA and TPA have three CH_2 groups, all in the same environment). What is interesting is that NON50-S50-Sol shows significantly weaker aromatic resonances than TAA or TPA, which suggests that the route to form these aromatic structures may rely on an amine activated reaction pathway, which NON does not have access to, and thus must use a kinetically slower route. NON50-S50-Sol also shows some alkene resonances, though they are comparatively weaker than those observed for TPA50-S50-Sol. These could be because that, as with TPA, NON's alkynes react progressively to an alkene and then to sp3 hybridised groups, but unlike TPA, because NON contains one fewer alkyne group, it a more complete reaction is observed due to there being proportionally less pi bonds for sulfur to react with in NON as compared to TPA. Much like the other Sol products, NON50-S50-Sol displays several broad peaks, reinforcing that the Sol products have a tendency to be less well defined than the Insols, and contain a wider variety of hydrogen environments. There are still some peaks present in Figure S25 that are analogous to those shown in the spectra of TPA and TAA polymers, for example the peak at 0.85 ppm which recurs in all the other ^{1}H NMR spectra. This indicates that despite the structural differences between TPA, TAA, and NON, they are all forming related products, which implies they are all accessing relatively similar reaction pathways. Once again, the ^{13}C NMR and DEPT135 ^{13}C NMR did not yield any signals through the noise for NON50-S50-Sol, though the ^{1}H ^{13}C HSQC did manage to produce a very weak ^{13}C NMR spectrum, though the HSQC itself is not of particular utility in understanding the polymer structure.

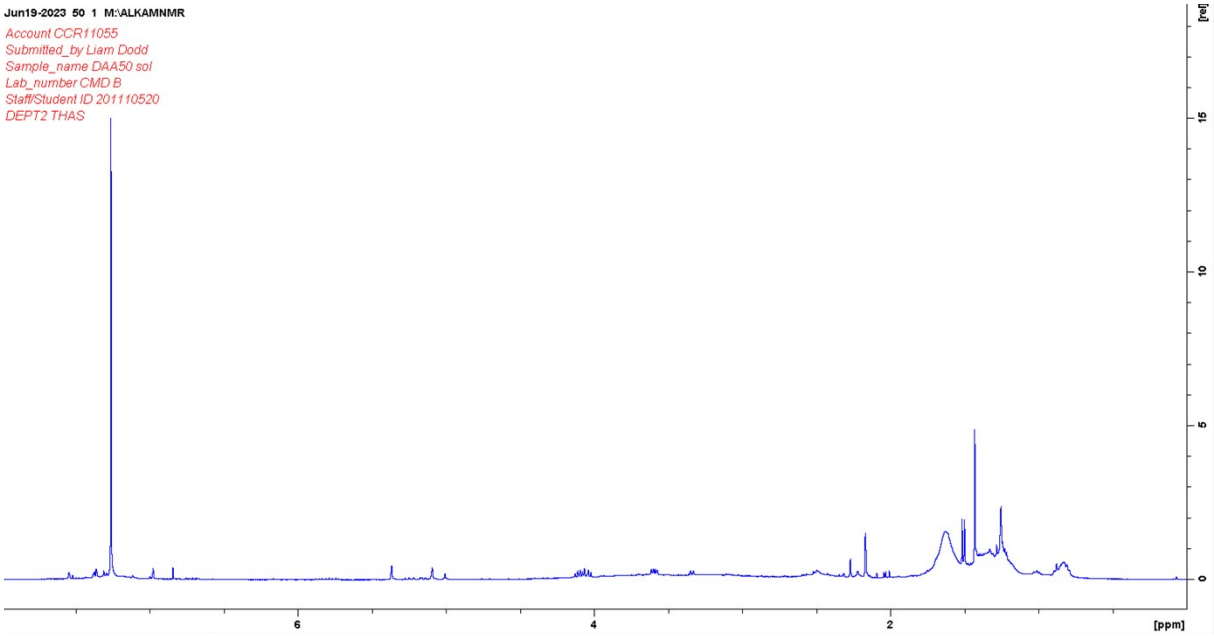

Figure S28: The ^{1}H NMR spectrum of the degradation products of DAA50-S50-Sol.

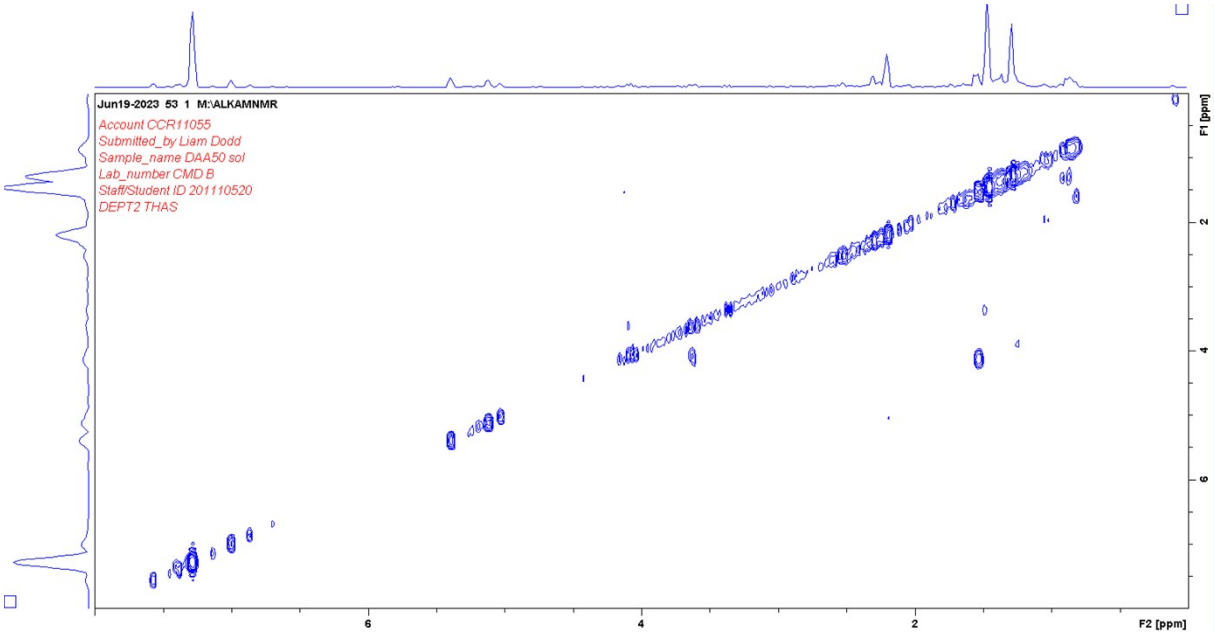

Figure S29: The ^{1}H ^{1}H COSY NMR spectrum of the degradation products of DAA50-S50-Sol.

The NMR spectra for DAA50-S50-Sol largely reinforce the conclusions drawn from the other spectra. Again, there is evidence of incomplete consumption of alkene bonds, suggesting that the Sol products are less well reacted and less well crosslinked in comparison to the Insol products. These alkene peaks are however quite weak, suggesting that for the most part, the reaction was close to completion. DAA50-S50-Sol displays no evidence of benzenes or phenols, much like TAA50-S50-Sol and TAA50-S50-Insol, again suggesting that alkenes are less effective at forming the aromatics by-products. Again, the intensity for the aromatic resonances are quite weak in comparison to the predominant sp3 region of the spectrum. As a Sol product DAA50-S50-Sol shows more numerous broad peaks, reinforcing the

conclusion that the Sol products are less well defined. Nevertheless, DAA50-S50-Sol does show similarities in its spectra as compared to the other polymers, such as the 0.85 ppm peak, again reinforcing that these polymers are utilising similar reaction pathways to form similar products. The ^{13}C NMR, DEPT135 ^{13}C NMR, and the ^{1}H ^{13}C HSQC NMR did not yield any signals through the noise for DAA50-S50-Sol.

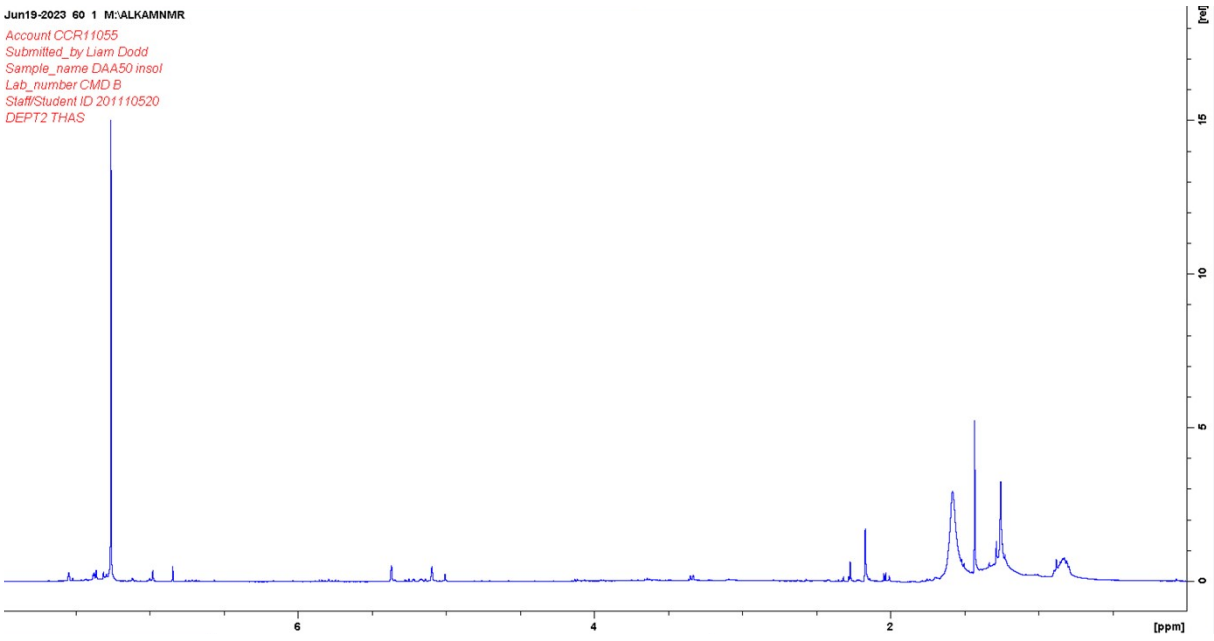

Figure S30: The ^{1}H NMR spectrum of the degradation products of DAA50-S50-Insol.

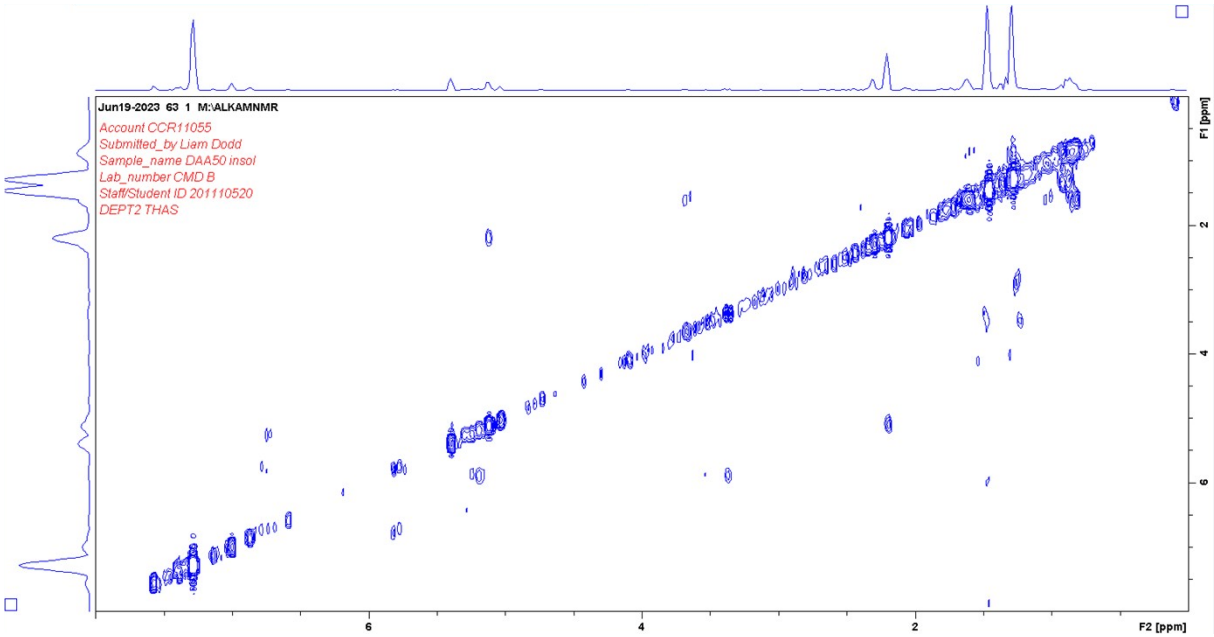

Figure S31: The ^{1}H ^{1}H COSY NMR spectrum of the degradation products of DAA50-S50-Insol.

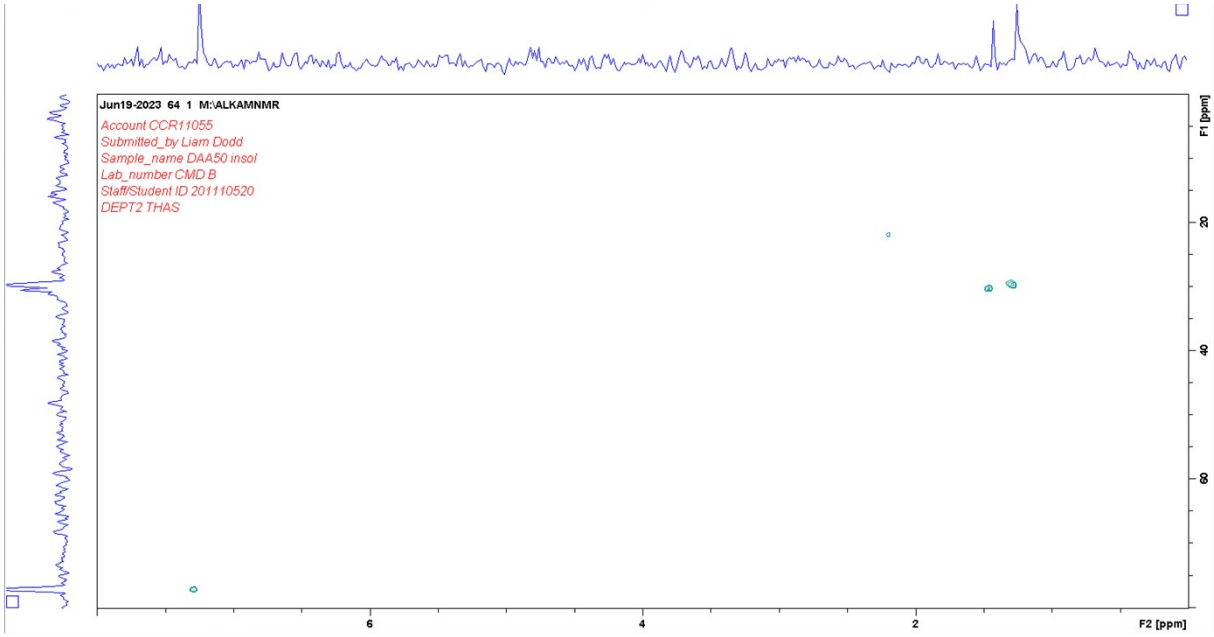

Figure S32: The ^{1}H ^{13}C HSQC NMR spectrum of the degradation products of DAA50-S50-Insol.

The spectra of DAA50-S50-Insol only reinforce the previous conclusions and do not add anything of note. Once again, the ^{13}C NMR and DEPT135 ^{13}C NMR did not yield any signals through the noise for DAA50-S50-Insol, though the ^{1}H ^{13}C HSQC did manage to produce a very weak ^{13}C NMR spectrum, though the HSQC itself is not of particular utility in understanding the polymer structure.

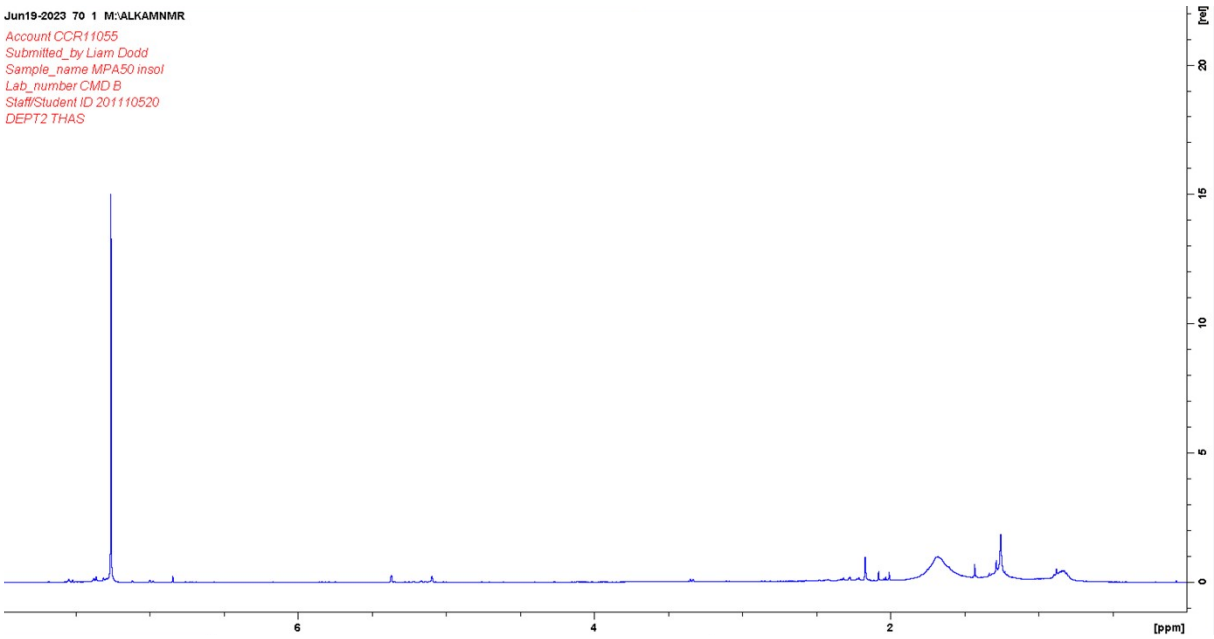

Figure S33: The ^{1}H NMR spectrum of the degradation products of MPA50-S50-Insol.

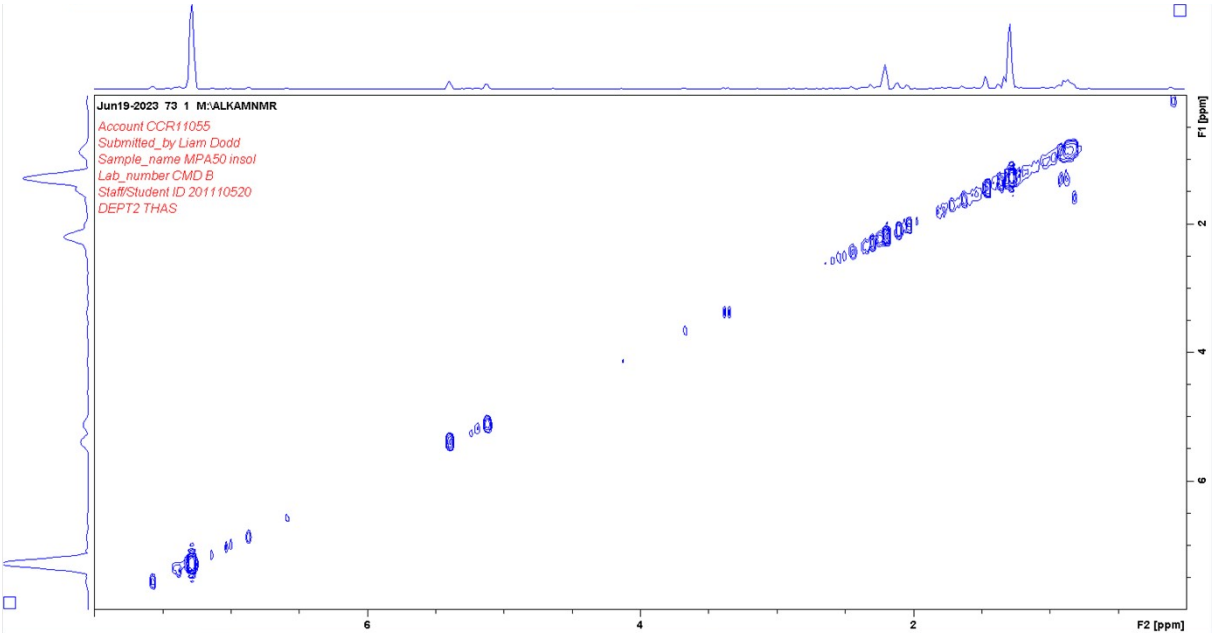

Figure S34: The ^{1}H ^{1}H COSY NMR spectrum of the degradation products of MPA50-S50-Insol.

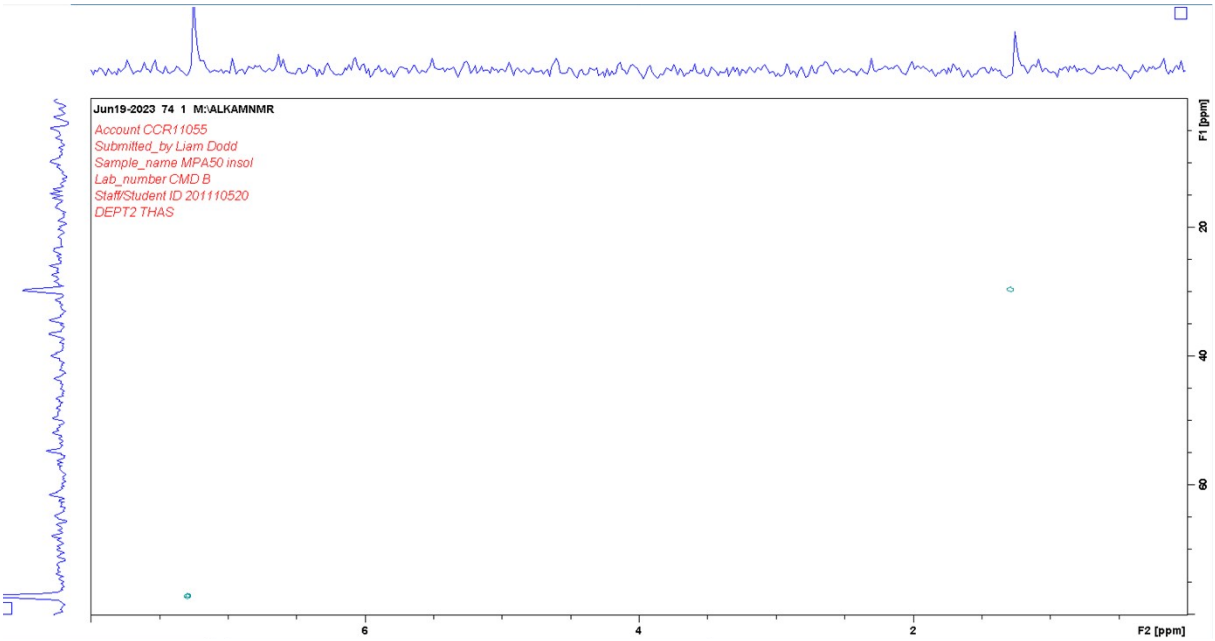

Figure S35: The ^{1}H ^{13}C HSQC NMR spectrum of the degradation products of MPA50-S50-Insol.

The spectra of MPA50-S50-Insol do not add any new conclusions of note, and only reinforce the already established conclusions. The only significant difference between the spectra of MPA50-S50-Insol and the other polymer spectra is that the spectrum is comparatively simple, owing to MPA's simple structure. Once again, the ^{13}C NMR and DEPT135 ^{13}C NMR did not yield any signals through the noise for MPA50-S50-Insol, though the ^{1}H ^{13}C HSQC did manage to produce a very weak ^{13}C NMR spectrum, though the HSQC itself is not of particular utility in understanding the polymer structure.

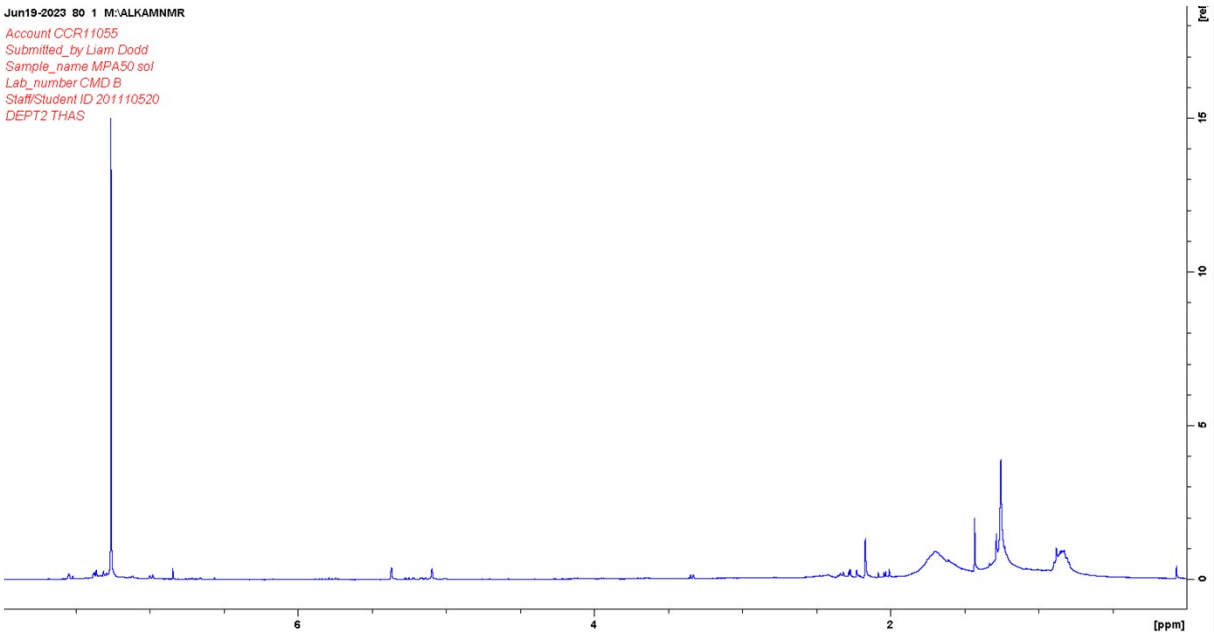

Figure S36: The ^{1}H NMR spectrum of the degradation products of MPA50-S50-Sol.

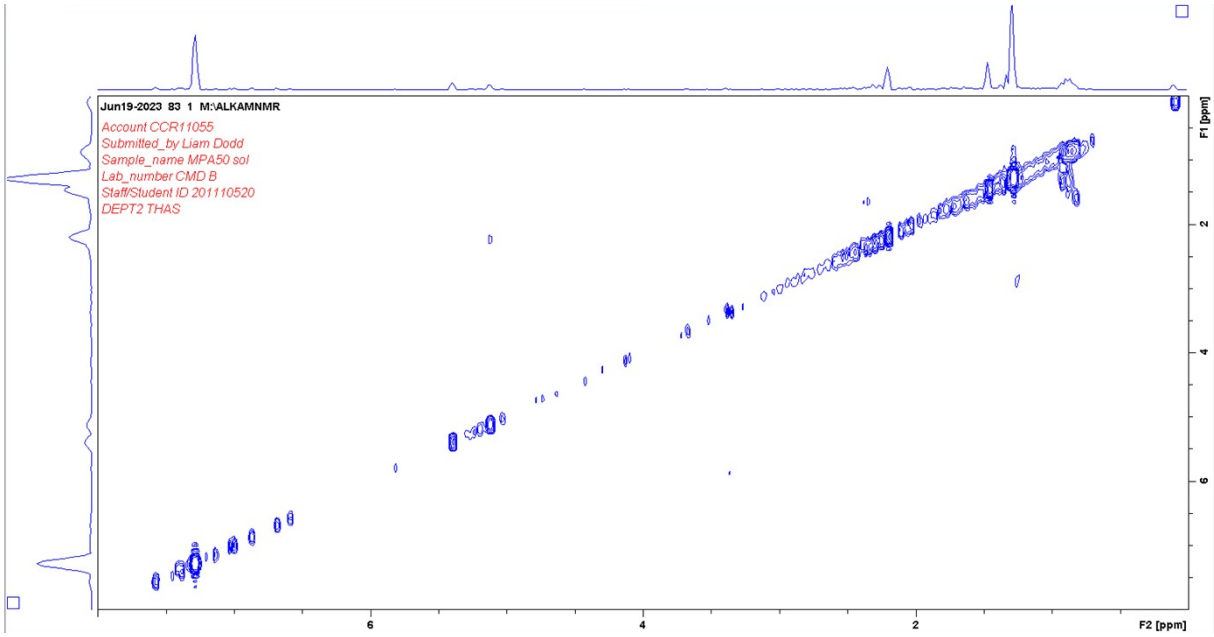

Figure S37: The ^{1}H ^{1}H COSY NMR spectrum of the degradation products of MPA50-S50-Sol.

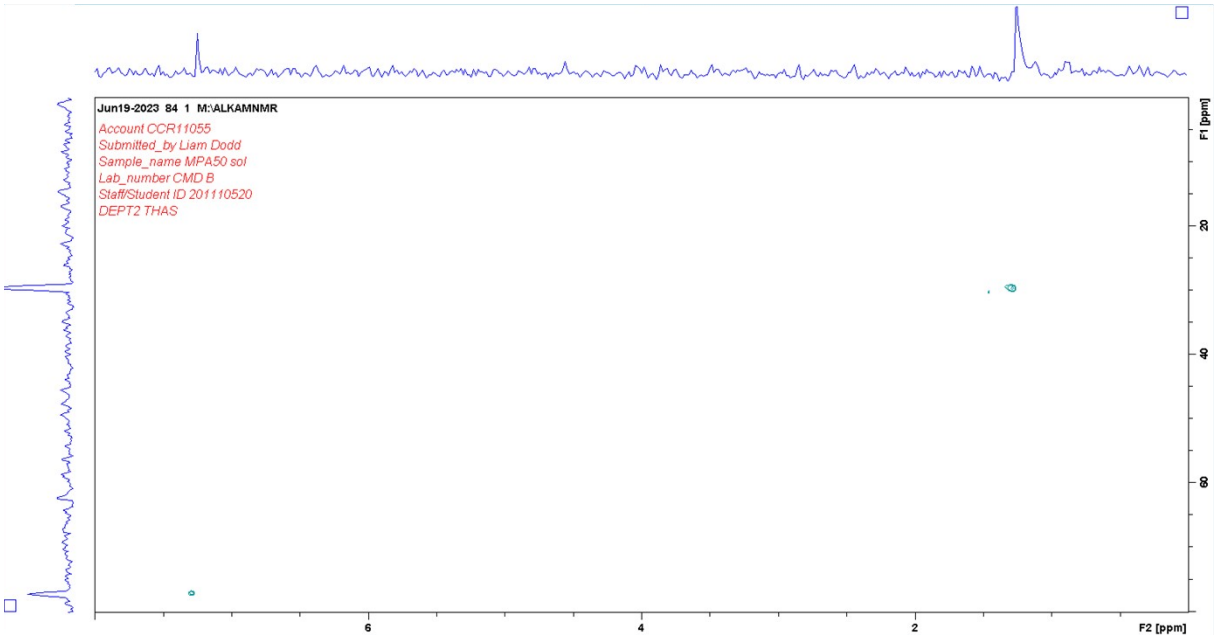

Figure S38: The ^{1}H ^{13}C HSQC NMR spectrum of the degradation products of MPA50-S50-Sol.

The spectra of MPA50-S50-Sol do not add any new conclusions of note, and only reinforce the already established conclusions. The only significant difference between the spectra of MPA50-S50-Sol and the other polymer spectra is that the spectrum is comparatively simple, owing to MPA's simple structure. Once again, the ^{13}C NMR and DEPT135 ^{13}C NMR did not yield any signals through the noise for MPA50-S50-Sol, though the ^{1}H ^{13}C HSQC did manage to produce a very weak ^{13}C NMR spectrum, though the HSQC itself is not of particular utility in understanding the polymer structure.

X. Antimicrobial Activity Method

Glycerol stocks of *S. aureus* strain USA300 were stored at −80 °C for long-term storage. For experimental use, frozen glycerol stocks of *S. aureus* were defrosted and spread onto LB agar plates which were then incubated overnight at 37 °C. Bacterial cultures were prepared by swabbing one colony into 10 mL of LB broth, followed by overnight incubation at 37 °C. Colony forming units (CFU) were enumerated by serially diluting the cultures in PBS onto LB agar, using the Miles and Misra method. CFU/cm^2 and CFU/mL were calculated using the following equation:

$$CFU = \frac{Number\ of\ Colonies \times Dilution\ Factor}{Volume\ of\ Culture\ Plate}$$

S. aureus USA300 was used to evaluate the antibacterial efficiency of the materials. Overnight cultured bacteria prepared in LB broth were diluted to 105 CFU/mL (OD600 = 0.001) in LB medium. 5 mg of powdered sample was added to 5 ml of diluted culture. Diluted culture in the absence of sample was used as an untreated control. The samples were incubated for 5 h at 37 °C on a roller. Viable cells were enumerated after serial dilution of the solution in PBS onto LB agar, using the Miles and Misra method.

XI. NMR Kinetics

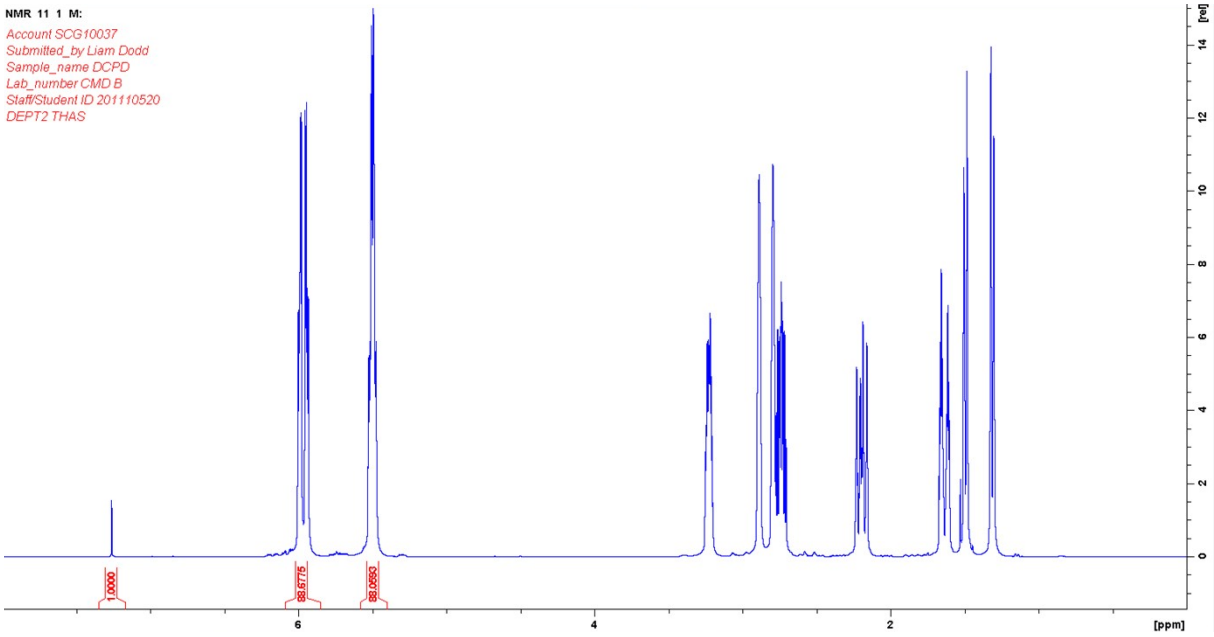

Figure S39: The ^{1}H NMR spectrum of DCPD in $CDCl_3$.

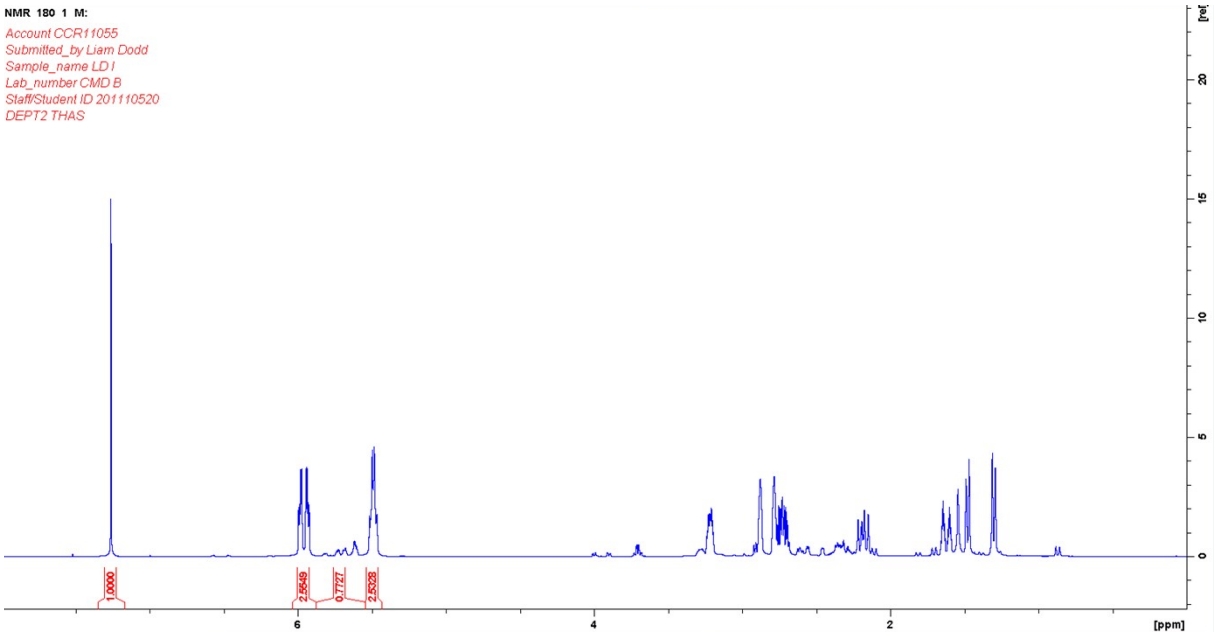

Figure S40: The ^{1}H NMR spectrum of an aliquot of a DCPD inverse vulcanisation reaction mixture in $CDCl_3$, taken at 60 minutes reaction time.

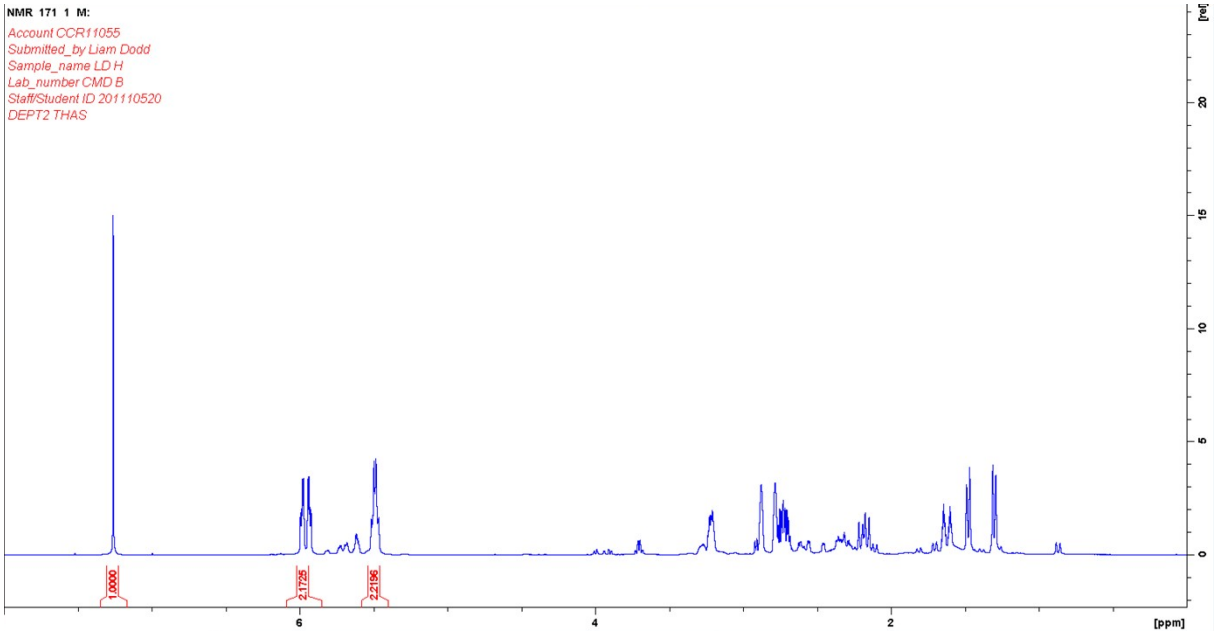

Figure S41: The ^{1}H NMR spectrum of an aliquot of a DCPD inverse vulcanisation reaction mixture in $CDCl_3$, taken at 90 minutes reaction time.

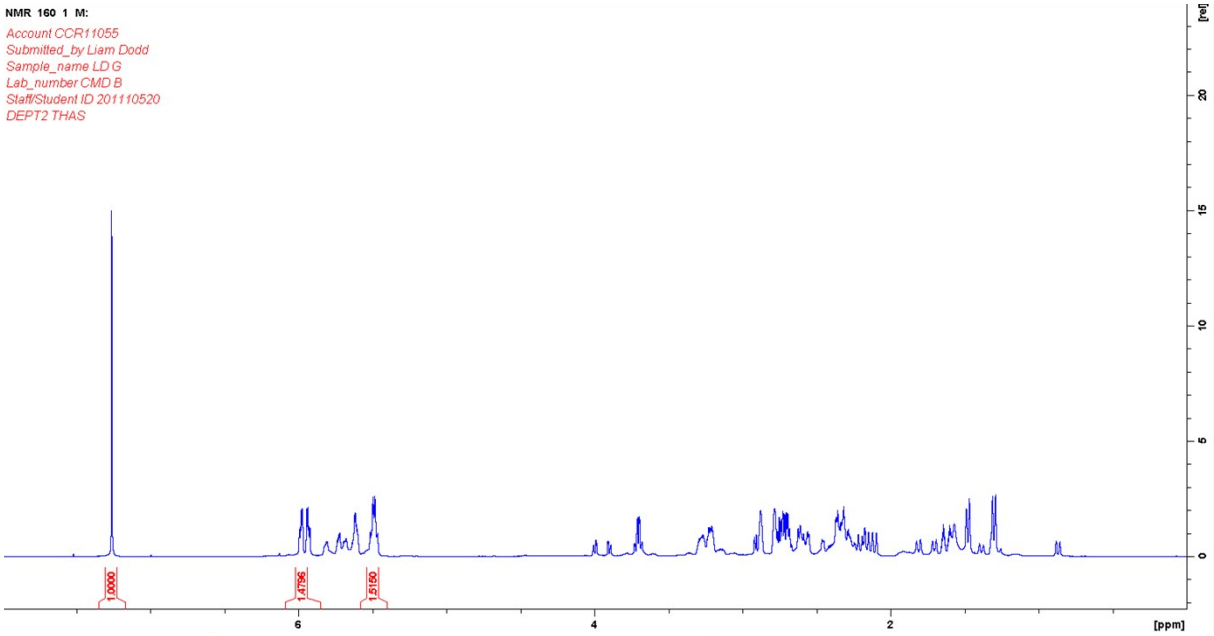

Figure S42: The ^{1}H NMR spectrum of an aliquot of a DCPD inverse vulcanisation reaction mixture in $CDCl_3$, taken at 120 minutes reaction time.